



HAL
open science

A Review on Numerical Modeling of the Hygrothermal Behavior of Building Envelopes Incorporating Phase Change Materials

Mohamed Sawadogo, Alexandre Godin, Marie Duquesne, Ameer El Amine Hamami, Rafik Belarbi

► **To cite this version:**

Mohamed Sawadogo, Alexandre Godin, Marie Duquesne, Ameer El Amine Hamami, Rafik Belarbi. A Review on Numerical Modeling of the Hygrothermal Behavior of Building Envelopes Incorporating Phase Change Materials. *Buildings*, 2023, 13 (12), pp.3086. 10.3390/buildings13123086 . hal-04337556

HAL Id: hal-04337556

<https://hal.science/hal-04337556v1>




Submitted on 12 Dec 2023

HAL is a multi-disciplinary open access archive for the deposit and dissemination of scientific research documents, whether they are published or not. The documents may come from teaching and research institutions in France or abroad, or from public or private research centers.

L'archive ouverte pluridisciplinaire **HAL**, est destinée au dépôt et à la diffusion de documents scientifiques de niveau recherche, publiés ou non, émanant des établissements d'enseignement et de recherche français ou étrangers, des laboratoires publics ou privés.

Review

A Review on Numerical Modeling of the Hygrothermal Behavior of Building Envelopes Incorporating Phase Change Materials

Mohamed Sawadogo^{1,2}, Alexandre Godin^{1,2}, Marie Duquesne¹, Ameer El Amine Hamami^{1,*}
and Rafik Belarbi^{1,3,*}

- ¹ LaSIE UMR CNRS 7356, La Rochelle Université, Avenue Michel Crépeau, CEDEX 1, 17042 La Rochelle, France; mohamed.sawadogo@univ-lr.fr (M.S.); alexandre.godin@univ-lr.fr (A.G.); marie.duquesne@univ-lr.fr (M.D.)
- ² 4ev Lab, EDF R&D, CNRS, LaSIE, La Rochelle University, Avenue Michel Crépeau, CEDEX 1, 17042 La Rochelle, France
- ³ Department of Architecture, Canadian University Dubaï, City Walk Dubaï, Dubai P.O. Box 415053, United Arab Emirates
- * Correspondence: ahamami@univ-lr.fr or ameur_el_amine.hamami@univ-lr.fr (A.E.A.H.); rafik.belarbi@univ-lr.fr (R.B.)

Abstract: Buildings are submitted to various external and internal solicitations that could affect its energy performance. Among these solicitations, temperature and moisture play a crucial role and could irrevocably affect the comfort of the occupants and the indoor air quality of the living environment. To assess the impact of the solicitation on building performance, a precise modeling of the heat, air, and moisture transfer phenomenon is necessary. This work proposes an extensive review of the hygrothermal models for building envelopes. The different models are divided into nodal and HAM techniques for heat, air, and moisture (HAM) transfer models. The HAM approach has been classified based on four driving potentials: moisture content, relative humidity, capillary pressure, and vapor pressure. Phase change materials (PCMs), alongside hygroscopic materials, enhance building thermal capacity and energy efficiency. There are various approaches to studying phase changes, with enthalpy-based and heat capacity approaches being the most popular. Building performance can be improved by combining PCM thermal inertia with hygroscopic moisture management. This review has exhibited the need for numerical models that address phase change and moisture behavior in these hybrid materials, capable of controlling temperature and humidity.

Keywords: heat, air, and moisture transfer; phase change materials; modeling; humidity; temperature control materials



Citation: Sawadogo, M.; Godin, A.; Duquesne, M.; Hamami, A.E.A.; Belarbi, R. A Review on Numerical Modeling of the Hygrothermal Behavior of Building Envelopes Incorporating Phase Change Materials. *Buildings* **2023**, *13*, 3086. <https://doi.org/10.3390/buildings13123086>

Academic Editor: Karim Ghazi Wakili

Received: 2 November 2023

Revised: 30 November 2023

Accepted: 7 December 2023

Published: 12 December 2023



Copyright: © 2023 by the authors. Licensee MDPI, Basel, Switzerland. This article is an open access article distributed under the terms and conditions of the Creative Commons Attribution (CC BY) license (<https://creativecommons.org/licenses/by/4.0/>).

1. Introduction

Energy conservation and environmental sustainability are major social concerns. They are linked to climate change phenomena, which, at the building level, result in uncomfortable conditions during the different seasons. Indeed, buildings are subjected to various internal and external solicitations that have an effect on their hygrothermal behavior. Inhabitant comfort and indoor air quality are both significantly impacted by these requests, and temperature and moisture play a crucial role [1,2]. This has led to the development of humidity control materials such as geo-based material [3–7] (rammed earth, cob earth material), bio-based material [8–11] (natural fiber components, straw, hemp), and generally the innovative ecofriendly materials. A better understanding of the properties of these materials and their response to dynamic climatic conditions constitutes a major challenge in order to improve their energy and environmental performance. Indeed, the relative humidity of the air can be automatically regulated by humidity control materials that rely on their own features and the induction of changes in the surrounding temperature and humidity. Therefore, a precise modeling of the heat, air, and moisture transport phenomenon

is required to determine the effect of the solicitation on building performances [12–20]. The mathematical model for expressing the quantity of moisture held in the material is a decisive issue among all the physical phenomena involved in heat and mass transfer processes through porous building materials.

To this end, the exploration of simultaneous heat and moisture transfer in porous building materials and envelopes has been a subject of research for over seven decades, resulting in the development of numerous theoretical models. The driving potentials and assumptions of each theoretical model are different, and there is no unified theoretical model to describe the heat transfer and moisture migration in building envelopes [21]. The most used and accepted macroscopic models for studying heat and moisture transfer through porous media are the Luikov model [22] and the Philip and de Vries model [23], which use the temperature and moisture content as driving potentials. However, the major limitation of using the moisture content profile as a driving potential is its discontinuity at the interface between two porous media [24]. In order to address this limitation, several models have been developed based on alternative driving potentials such as relative humidity [25], capillary pressure [26], vapor pressure [22], and porous matrix potential [27].

In addition, phase change materials (PCMs) has been identified as an efficient technique to increase the thermal capacity, energy performance, and comfort impact of buildings [28–33]. During the phase change process, PCMs absorb or release large amounts of latent heat from or to the indoor air. In this way, PCMs can smooth the temperature fluctuations and increase the thermal inertia of buildings. The variety of materials available, material liability and safety, cost and economic viability, design configurations, integration with other sustainable energy technologies, and impact on thermal and energy performance are just a few of the challenges associated with using PCMs in buildings [34]. To address these challenges, numerical simulation is seen as an effective solution and has been used in numerous studies. There are several different approaches available for studying solid–liquid phase change. These include enthalpy-based methods, effective heat capacity methods, front tracking methods, and adaptive grid methods [35]. However, a particular numerical strategy should be carefully chosen in order to evaluate accurately the performance of buildings incorporating PCMs.

PCMs and hygroscopic materials can be combined to improve the performance of building envelopes as a whole [36,37]. Energy efficiency, temperature regulation, and moisture control can all be improved at once by combining the thermal inertia of PCMs with the moisture inertia of hygroscopic materials. Nevertheless, research in this field has primarily focused on thermal and energy factors, frequently ignoring the equally important hydric performance, despite the potential advantages of such integrated materials. Only a few researchers have thus thoroughly investigated both thermal and hygroscopic behavior inside these integrated systems.

This last concern has motivated the present study, which aims at reviewing the hygrothermal model to evaluate the performances of building materials incorporating PCMs. The study's novelty hinges on two key aspects:

- the classification of hygrothermal models based on their driving potential.
- the integration of phase change materials (PCMs) models into these hygrothermal frameworks.

First, the different models of heat, air, and moisture (HAM) transfer in buildings are presented. These models are divided into two groups, namely the nodal and the HAM approach. In the HAM, the models are divided based on four driving potentials: moisture content, relative humidity, capillary pressure, and vapor pressure. Afterwards, the numerical models of PCMs in buildings are presented with a focus on the so-called fixed domain method that is widely used in the literature. Finally, models that integrate both hygrothermal and phase change models are presented, and the limitations as well as the challenges of the different models are discussed.

2. Physical Phenomena of Heat, Air, and Moisture Transfer

Heat, air, and moisture transfer remains a highly complex phenomenon, requiring detailed modeling that takes into account not only each individual phenomenon but also all the interactions between the different phenomena. All these equations are based on the fundamental principle of heat and mass conservation. In this section, the equations describing each phenomenon are presented separately, before introducing the various models reported in the literature that translate the coupling between different phenomena.

2.1. Moisture Transfer

Moisture refers to the transfer of water in liquid and vapor forms. This moisture (water and vapor) comes from several sources: rainwater running down walls, water vapor present in the material's ambient air, etc. [24]. It can be absorbed by porous building envelopes, depending on the equilibrium sorption moisture content.

2.1.1. Liquid Water Transfer

The transfer of the liquid phase is described by Darcy's law and is induced by a capillary suction gradient [23,38]. The mass flow density of liquid water is obtained by applying Darcy's law as follows:

$$J_{lc} = -\rho_l K_l \nabla \psi \quad (1)$$

where K_l is the hydraulic conductivity [$\text{m}\cdot\text{s}^{-1}$], ρ_l the liquid density [$\text{kg}\cdot\text{m}^{-3}$], and ψ [m] the capillary suction. Liquid water can also migrate under the effect of gravity [25], which leads to the consideration of an additional J_{lg} [$\text{kg}\cdot\text{m}^{-2}\cdot\text{s}^{-1}$] flow term on top of the previous term:

$$J_{lg} = -\rho_l K_l \vec{k} \quad (2)$$

where \vec{k} is the vertical unit vector oriented positively upwards.

It is also possible to use other transfer motors to express liquid water flow, such as water content, relative humidity, and vapor pressure. For example, Crausse et al. [38] defined a flux expression as a function of water content (θ [$\text{kg}\cdot\text{m}^{-3}$]) as follows:

$$J_{lc} = -\rho_l (D_{\theta l} \nabla \theta + D_{Tl} \nabla T) \quad (3)$$

where $D_{\theta l}$ [$\text{m}^2\cdot\text{s}^{-1}$] and D_{Tl} [$\text{m}^2\cdot\text{s}^{-1}\cdot\text{K}^{-1}$] represent the diffusion coefficients of liquid water under the effect of a water content gradient and a temperature gradient, respectively.

These water diffusivities are related to hydraulic conductivity by:

$$D_{\theta l} = K_l \left(\frac{\partial \psi}{\partial \theta} \right)_T \quad (4)$$

$$D_{Tl} = K_l \left(\frac{\partial \psi}{\partial T} \right)_\theta \quad (5)$$

2.1.2. Water Vapor Transfer

Water vapor is transported by diffusion under the influence of a concentration gradient. The molecular diffusion process of water vapor in air is given as a function of the vapor concentration gradient by Fick's law [39] as follows:

$$J_v = -D_v \nabla \rho_v \quad (6)$$

with:

J_v , the water vapor mass flux density [$\text{kg}\cdot\text{m}^{-2}\cdot\text{s}^{-1}$];

D_v , the coefficient of vapor diffusion in air [$\text{m}^2\cdot\text{s}^{-1}$], characterizing the movement resulting from diffusion.

$\nabla\rho_v$, the water vapor concentration gradient.

If we consider water vapor pressure as the driving force for moisture transfer, Fick's law can be written as a function of the vapor pressure gradient:

$$p_v = \rho_v r_v T \leftrightarrow \rho_v = \frac{p_v}{r_v T} \quad (7)$$

$$J_v = \frac{D_v}{r_v T} \nabla p_v \quad (8)$$

where p_v [Pa] is the water vapor pressure and r_v [$\text{J.kg}^{-1}.\text{K}^{-1}$] is the ideal gas constant.

2.2. Air Transfer

In the presence of a total pressure gradient, a transfer of dry and humid air through an infiltration process occurs and must be taken into account in the total balance. This phenomenon, which is governed by a total pressure gradient, is expressed as follows:

$$J_a + J_v = -k_f \nabla P \quad (9)$$

with: J_a , the dry and humid air mass flux density [$\text{kg.m}^{-2}.\text{s}^{-1}$];

k_f , the total infiltration coefficient [$\text{kg.m}^{-1}.\text{s}^{-1}.\text{Pa}^{-1}$];

P , the total pressure [Pa].

Some others, such as Tariku et al. [40], used Poiseuille's law of proportionality [41], which relates the pressure gradient to flow velocity to express the airflow through a porous media. Under the assumption of incompressible air due to the very low airflow speeds and low pressure and temperature changes that are encountered in practice, the conservation equation for air mass balance is given by:

$$\nabla(\delta_a \nabla P) = 0 \quad (10)$$

where δ_a is the air permeability [s].

2.3. Heat Transfer

In a porous material partially saturated with water, heat transfer can take place in three forms: purely conductive transfer according to Fourier's law [42], convective transfer of sensible heat by liquid and vapor flows, and, finally, transfer of latent heat carried by the vapor. Considering all these phenomena, the heat flux density can be written as follows:

$$J_q = -\lambda \nabla T + h_l (J_{lc} + J_{lg}) + h_v J_v \quad (11)$$

with λ [$\text{W.m}^{-1}.\text{K}^{-1}$] the material's heat conductivity, and h_l and h_v [J.kg^{-1}] the enthalpy of mass of liquid water and vapor, respectively.

Remember that at a given temperature T [K] and with respect to a reference temperature T_0 , these two quantities can be written as:

$$h_l = C_l (T - T_0) \quad (12)$$

$$h_l = C_l (T - T_0) + h_{lv} \quad (13)$$

with C_l [$\text{J.kg}^{-1}.\text{K}^{-1}$] the liquid water heat capacity and h_{lv} [J.kg^{-1}] the latent heat of vaporization of water.

3. Coupled Heat, Air, and Moisture Transfer

The study of coupled heat, air, and moisture transfer in porous materials is of key importance in a variety of fields, including building science, materials engineering, and environmental science. Porous materials, such as building components and soils, often undergo complex interactions between heat, air, and moisture, resulting in complex

hygrothermal behaviors. To understand and predict these behaviors, researchers have developed a plethora of models, each tailored to specific scenarios and assumptions. Two different approaches are used to predict coupled heat, air, and moisture transfer in porous materials: nodal models and HAM models.

3.1. Nodal Approach

In the nodal approach, each node represents volumes of material or components, while inter-node connections represent the flow paths of thermal and mass fluxes (walls, doors, windows, etc.). The graphic representation of the model has the same appearance as an electrical diagram; hence, the analogue method was used, where:

- the temperature and density of water vapor are represented by electrical potentials;
- energy flows and mass transfers are represented by current intensities;
- thermal and moisture resistances are represented by electrical resistances;
- the thermal and moisture retention capacities are represented by capacitors.

The nodal approach is a one-dimensional approach that is currently employed in the most common Building Energy Simulation (BES) software, such as TRNSYS, Energy-Plus [43]. They all focus on describing the dynamic changes in indoor relative humidity and temperature, which occur due to variations in outdoor climate, hygrothermal loads, and the moisture buffering effect of indoor condition loads.

Boyer et al. [44] described a physical model of the building that is obtained by assembling thermal models of each element such as walls and glass windows. The thermo-convective balance equation of the dry-bulb air node and the radiative balance equation of the inside mean radiant temperature node are considered in the proposed model. The mathematical formulation of the thermal model of the building is a linear system of four equations expressed as follows:

$$C_{si} \frac{dT_{si}}{dt} = h_{ci}(T_{ai} - T_{si}) + h_{ri}(T_{rm} - T_{si}) + K(T_{se} - T_{si}) + q_{swi} \quad (14)$$

$$C_{se} \frac{dT_{se}}{dt} = h_{ce}(T_{ai} - T_{se}) + h_{re}(T_{sky} - T_{se}) + K(T_{se} - T_{si}) + q_{swe} \quad (15)$$

$$C_{ai} \frac{dT_{ai}}{dt} = \sum_{j=1}^{N_w} h_{ci}(T_{ai} - T_{si}(j)) + c\dot{Q}(T_{ae} - T_{ai}) \quad (16)$$

$$0 = \sum_{j=1}^{N_w} h_{ci} A_j (T_{si}(j) - T_{rm}) \quad (17)$$

where C [$\text{J.K}^{-1}.\text{m}^{-2}$] is the thermal capacity, c [$\text{J.kg}^{-1}.\text{K}^{-1}.\text{m}^{-2}$] is the specific heat capacity, h [$\text{W.m}^{-2}.\text{K}^{-1}$] is the heat transfer coefficient, K [$\text{W.m}^{-2}.\text{K}^{-1}$] is the thermal conductivity per unit of length, q [W.m^{-2}] the radiation flux density, \dot{Q} [kg.s^{-1}] is the mass flow rate, and A [m^2] is the area.

The subscripts *ae*, *ai*, *se*, *si*, *ce*, *ci*, *lwe*, *re*, *ri*, *rm*, *swe*, *swi*, *w* stand for air exterior, air interior, surface exterior, surface interior, exterior convection, interior convection, long wave exterior, exterior radiation, interior radiation, inside radiant mean, short wave exterior, short wave interior, and wall, respectively.

Except WUFI, which integrates a full moisture model, most of the building energy simulation software such as TRNSYS and EnergyPlus primarily focuses on simulating temperature variations and energy requirements in specific spaces on a large scale [43]. As a consequence, in these tools, the moisture exchange models at the wall scale rely on a simplified approach that does not account for the coupling of heat and moisture transfer phenomena through the building envelope.

One can distinguish two simplified models for simulating surface moisture adsorption and desorption: the Effective Capacitance Moisture (ECM) model and the Effective Moisture Penetration Depth (EMPD) model [45].

An effective moisture capacitance, defined as the product of the zone air mass and a moisture capacitance ratio, is used in the first model to account for the buffer effect of adsorptive and desorptive materials, soil areas, or plants [45]. A moisture balance for any zone results in the following differential equation:

$$M_{air,i} W_{cap} \frac{d\omega_i}{dt} = \dot{m}_{inf,i} (\omega_a - \omega_i) + \sum_k^{nvent} \dot{m}_{v,k,i} (\omega_{v,k,i} - \omega_i) + \dot{W}_{g,i} + \sum_{surfaces}^{i-j} \dot{m}_{cp\ lg,s} (\omega_j - \omega_i) \quad (18)$$

with $M_{air,i}$ [kg], the effective moisture capacitance of the zone;

W_{cap} , the humidity capacitance of the air and ranges from 1 to 10;

ω_i [%], the humidity ratio of the zone;

ω_a [%], the ambient humidity ratio;

$\omega_{v,k,i}$ [%], the humidity ratio of the ventilation air from ventilation type k;

$\dot{W}_{g,i}$ [kg.s⁻¹], internal moisture gains;

ω_j [%], the humidity ratio of an adjacent zone j;

$\dot{m}_{inf,i}$ [kg.s⁻¹], the mass flow rate of infiltration air;

$\dot{m}_{v,k,i}$ [kg.s⁻¹], the mass flow rate of ventilation air of ventilation type k;

$\dot{m}_{cp\ lg,s}$ [kg.s⁻¹], the mass flow rate of air entering zone i across walls or windows.

The buffer storage humidity model describes a separate humidity buffer divided into surface and deep storage. Each buffer is defined by three parameters: the gradient of the sorptive isothermal line of the material (κ), the mass of the material (M), and the moisture exchange coefficient between the two regions (β) and the zone air (Equation (19)).

$$M_{air,i} \frac{d\omega_i}{dt} = \dot{m}_{inf,i} (\omega_a - \omega_i) + \sum_k^{nvent} \dot{m}_{v,k,i} (\omega_{v,k,i} - \omega_i) + \dot{W}_{g,i} + \sum_{surfaces}^{i-j} \dot{m}_{cp\ lg,s} (\omega_j - \omega_i) + \beta_{surf} (\omega_{surf} - \omega_i) \quad (19)$$

Additionally, two new differential equations were introduced to describe the dynamics of the water content of the surface and the deep storage.

$$M_{surf} \kappa_{surf} f(\varphi, \omega) \frac{d\omega_{surf}}{dt} = \beta_{surf} (\omega_i - \omega_{surf}) + \beta_{deep} (\omega_{deep} - \omega_{surf}) \quad (20)$$

$$M_{deep} \kappa_{deep} f(\varphi, \omega) \frac{d\omega_{deep}}{dt} = \beta_{deep} (\omega_{surf} - \omega_{deep}) \quad (21)$$

κ_{surf} [kg water/kg material/rel. humidity], the gradient of sorptive isothermal line of surface buffer;

κ_{deep} [kg water/kg material/rel. humidity], the gradient of sorptive isothermal line of deep buffer;

$f(\varphi, \omega)$, the conversion factor from relative humidity to humidity ratio;

β_{surf} [kg.s⁻¹], the exchange coefficient between zone and surface storage;

β_{deep} [kg.s⁻¹], the exchange coefficient surface between storage and deep storage.

It should be noted that this model allows taking into account the moisture transfer between external walls, internal walls, or furniture and the zone air only. No moisture transfer with the exterior is modeled; as a result, the outdoor climate has no effect on the moisture transfer within the building envelope [46,47]. This limitation has led authors to develop fully coupled models based on the conservation principle (heat and mass).

3.2. Heat, Air, and Moisture Conservation Based Models

HAM models offer a more complex approach to understand the coupled transfer of heat, air, and moisture. Unlike the nodal approach, HAM models take into account the simultaneous movement of heat, air, and moisture within porous materials. These models integrate various physical processes such as conduction, convection, capillarity, and vapor diffusion. One of the key factors differentiating these models is the choice of transfer motors they take into account. Heat, air, and moisture can move through porous materials by different mechanisms, such as conduction, convection, and capillarity. A summary of the different models based on their driving potential is presented in Table 1.

Table 1. Summary of the different models based on their driving potential.

Driving Potential	References
Moisture content	[15,23,24,26,48–58]
Relative humidity	[25,59–73]
Capillary pressure	[74–80]
Vapor pressure	[81–85]

3.2.1. Models Using Moisture Content as Driving Potential

The first coupled heat and moisture models were developed in 1957 by Philip and de Vries [23]. This model was based on the hypothesis of temperature-dependent soil moisture transport. Volumetric water content θ [$\text{m}^3 \cdot \text{m}^{-3}$] and temperature T [K] are the main driving forces of transport for heat and moisture transfer. The general differential equations describing coupled heat and moisture transfer in porous materials are:

$$\frac{\partial \theta}{\partial t} = \nabla(D_{\theta} \nabla \theta) + \nabla(D_T \nabla T) + \frac{\partial K}{\partial z} \quad (22)$$

$$\rho_s C_p \frac{\partial T}{\partial t} = \nabla(\lambda \nabla T) + h_{lv} \nabla(D_{v\theta} \nabla \theta) \quad (23)$$

where ρ_s [$\text{kg} \cdot \text{m}^{-3}$] is the density of the material, C_p [$\text{J} \cdot \text{kg}^{-1} \cdot \text{K}^{-1}$] is the specific heat of the dry material, λ [$\text{W} \cdot \text{m}^{-1} \cdot \text{K}^{-1}$] is the thermal conductivity of material, h_{lv} [$\text{J} \cdot \text{kg}^{-1}$] is the latent heat of evaporation, $D_{v\theta}$ [$\text{m}^2 \cdot \text{s}^{-1}$] is the isothermal water vapor diffusion coefficient, K [$\text{m} \cdot \text{s}^{-1}$] is the hydraulic conductivity, and D_{θ} [$\text{m}^2 \cdot \text{s}^{-1}$] and D_T [$\text{kg} \cdot \text{m}^{-1} \cdot \text{s}^{-1} \cdot \text{K}^{-1}$] are, respectively, the moisture diffusion coefficient related to temperature and moisture content gradients.

Luikov et al. [48] was one of the first researchers to develop a mathematical model of thermo-hydric transfer in porous building materials. In this model, moisture in either vapor or liquid phase is transported under the influence of gradients in temperature, mass water content (u [$\text{kg} \cdot \text{kg}^{-1}$]), and total pressure. However, it proposes to separate liquid (j_l) and vapor flow (j_v), since a concentration gradient and the latter induce the former by a thermal gradient.

$$j_v = -D_v \rho_s \nabla u - D_{vT} \rho_s \nabla T \quad (24)$$

$$j_l = -D_l \rho_s \nabla u - D_{lT} \rho_s \nabla T \quad (25)$$

where D_v and D_l are the diffusion coefficients for water vapor and liquid water due to water content gradient, respectively.

D_{vT} and D_{lT} are the diffusion coefficients for water vapor and liquid water due to temperature gradient, respectively.

Luikov introduced the concept of phase change criterion (PCC) ε that is defined as the ratio of the water vapor flux divergence to the total moisture flux divergence, as shown in Equation (26).

$$\varepsilon = \frac{\text{div}(j_v)}{\text{div}(j_v) + \text{div}(j_l)} \quad (26)$$

In addition to the heat and mass conservation equation, Luikov proposed an additional equation to describe the total pressure variation. The system of heat, air, and moisture equation becomes:

$$\frac{\partial u}{\partial t} = \nabla \left(D_m \left(\nabla u + \delta_T \nabla T + \delta_f \nabla p \right) \right) \quad (27)$$

$$\rho_s C_p \frac{\partial T}{\partial t} = \nabla \left(\varepsilon h_{lv} D_m \nabla u + (\lambda + \varepsilon h_{lv} D_m \delta_T) \nabla T + \varepsilon h_{lv} D_m \rho_a \nabla p \right) \quad (28)$$

$$\rho C_f \frac{\partial p}{\partial t} = \nabla \left(\varepsilon D_m \nabla u - \varepsilon D_m \delta_T \nabla T + (k_f - \varepsilon D_m \rho_a) \nabla p \right) \quad (29)$$

where D_m [$\text{m}^2 \cdot \text{s}^{-1}$] is the moisture diffusion coefficient (water vapor and liquid water), δ_T [$\text{kg} \cdot \text{m}^{-3} \cdot \text{K}^{-1}$] is the thermogradient coefficient, C_f [Pa^{-1}] is the humid air capacity, k_f [$\text{kg} \cdot \text{m}^{-1} \cdot \text{s}^{-1} \cdot \text{Pa}^{-1}$] is the filtration permeability coefficient, and ρ_a [$\text{kg} \cdot \text{m}^{-3}$] is the air density.

The disadvantage of this model is that the parameter ε is not derived from experimental tests, and its empirical determination is complex. Irudayaraj and Wu [49] and Lewis and Ferguson [50] were the first who have numerically investigated the solution of Luikov's partial differential equations. This model has been used intensively by authors in the literature and has inspired many other models.

The moisture content is discontinuous at the interface between two materials due to their different hygroscopic properties, which brought problems when the model of multilayer materials was numerically solved. In order to solve the problem of moisture content discontinuity, the Luikov model and Philip–de Vries model had been modified by using other moisture driving potentials instead of the moisture content [26].

Mendes et al. [51,52] proposed a new hygrothermal model based on Philip and de Vries' equations, but instead of the volumetric water content, they preferred the volumetric moisture content θ and the temperature gradient T as the principal driving forces for the coupled heat and moisture transfer. The governing partial differential equations to model the hygrothermal behavior are therefore given by:

$$\frac{\partial \theta}{\partial t} = -\nabla (D_\theta \nabla \theta + D_T \nabla T) \quad (30)$$

$$\rho_s C_p \frac{\partial T}{\partial t} = \nabla (\lambda \nabla T) - h_{lv} \nabla (D_{v\theta} \nabla \theta + D_{vT} \nabla T) \quad (31)$$

Whitaker [53] proposed a detailed theory based on local mean volume behavior, in which the transport equations are described for each phase (solid, liquid, and gas) at macroscopic and microscopic levels.

$$\rho_s \frac{\partial u}{\partial t} = -\nabla (\rho_s f D_v \nabla u_v + D_b \nabla \rho_v - \rho_l \bar{V}_l) \quad (32)$$

$$= \nabla \left(\lambda \nabla T \right) + h_v \rho_g f D_v \nabla u_v + h_b D_b \nabla \rho_v - h_l \rho_l \bar{V}_l \quad (33)$$

where ρ_l , ρ_v , and ρ_s are, respectively, the density of water vapor, liquid phase, and solid phase, f is the dimensionless diffusivity tensor, u_v is the vapor mass fraction. D_v [$\text{m}^2 \cdot \text{s}^{-1}$] and D_b [$\text{m}^2 \cdot \text{s}^{-1}$] are, respectively, the water vapor and bound water diffusivity, and \bar{V}_l [$\text{m} \cdot \text{s}^{-1}$] is the liquid phase velocity [43,86], h_l , h_v , h_s , and h_b are, respectively, the enthalpy of the liquid phase, vapor phase, solid phase of water, and enthalpy of bound water. ε_l , ε_v , and ε_s are, respectively, the volume fraction of liquid, vapor, and solid.

Milly [54] have reformulated the Philip and de Vries equations for coupled heat and moisture transfer to obtain a "porous matrix potential" rather than moisture content as an independent variable.

Abahri et al. [55] proposed a more detailed model of coupled HAM transfer in building envelopes. For moisture transfer, in addition to diffusion, the contribution of the total pressure gradient, expressed by a coefficient, is taken into account, as is the contribution

of the thermal gradient expressed by a thermogradient coefficient. Both coefficients have been evaluated experimentally using laboratory tests [81]. The mass and energy balances are presented in the following system of equations:

$$\frac{\partial u}{\partial t} = \nabla (D_m (\nabla u + \delta_T \nabla T + \alpha_p \nabla p)) \quad (34)$$

$$C_p \rho_s \frac{\partial T}{\partial t} = \nabla (a_T \nabla T + \delta_u \nabla u + \alpha_T \nabla p) + \rho_s h_{lv} \varepsilon \frac{\partial u}{\partial t} \quad (35)$$

$$C_f \rho_s \frac{\partial p}{\partial t} = \nabla (k_f \nabla p) + \rho_s \varepsilon \frac{\partial u}{\partial t} \quad (36)$$

where a_T [$\text{W}\cdot\text{m}^{-1}\cdot\text{K}^{-1}$] is the modified thermal conductivity; δ_u [$\text{W}\cdot\text{m}^{-1}$] and α_T [$\text{W}\cdot\text{m}^{-1}\cdot\text{Pa}^{-1}$] are coefficients reflecting thermal advection due to moisture and total pressure gradients, respectively.

Similarly, Trabelsi et al. [15,57,58] proposed another macroscopic model based on Luikov's work, with temperature and vapor content as transfer drivers. The results of this model showed good agreement between numerical and analytical resolutions. In the same work, they studied the sensitivity of this model to the thermal gradient coefficient. This study showed the need to take thermo-diffusion into account, as its impact on overall mass transfer is non-negligible.

Qin et al. [24] proposed a dynamic mathematical model for simulating the coupled heat and moisture migration through multilayer porous building materials. Vapor content (v [$\text{kg}\cdot\text{m}^{-3}$]) and temperature were chosen as the principal driving potentials. The phase change occurring within porous materials acts as a heat source or sink, which results in the coupled relationship between moisture and heat transfer. The heat of absorption or desorption is generally one of the sources or sinks as well. Both phenomena are considered in the developed model. A local thermodynamic equilibrium between the fluid and the porous matrix is assumed. The set of differential equations for coupled heat and mass transfer are as follows:

$$\rho_s \zeta \frac{\partial v}{\partial t} = \nabla (D_m \nabla v) + \nabla (\varepsilon D_m \nabla T) \quad (37)$$

$$\rho_s C_p \frac{\partial T}{\partial t} = \nabla (\lambda \nabla T) + \rho_s \zeta (\varepsilon h_{lv} + \gamma) \frac{\partial v}{\partial t} \quad (38)$$

where ζ [$\text{m}^3\cdot\text{kg}^{-1}$] is the specific moisture storage capacity, and γ [$\text{J}\cdot\text{kg}^{-1}$] is the heat of absorption or desorption.

In addition, the authors proposed an analytical method [56] to calculate the coupled heat and moisture transfer process in building materials. The coupled system was first subjected to Laplace transformation, and then the equations were solved by introducing the Transfer Function Method. The transient temperature and moisture content distribution across the material can thus be easily obtained from the solutions. A new experimental methodology for determining the temperature gradient coefficient for building materials was also proposed [87]. Both the moisture diffusion coefficient and the temperature gradient coefficient for building material were experimentally evaluated.

3.2.2. Models Using Relative Humidity as Driving Potential

In 1995, Künzel introduced a new model that was based on Kieβl's theorem [25]. In this model, Künzel attempted to use the terms of relative humidity φ and temperature T as the primary driving forces to describe the coupled heat and moisture transfer in building components.

$$\frac{dw}{d\varphi} \frac{d\varphi}{dt} = \nabla (D_\varphi \nabla \varphi + \delta_v \nabla (\varphi p_{sat})) \quad (39)$$

$$\frac{dH}{dT} \frac{dT}{dt} = \nabla (\lambda \nabla T) + h_{lv} \nabla (\delta_v \nabla (\varphi p_{sat})) \quad (40)$$

where $\frac{dw}{d\varphi} = C_m$ [kg.m⁻³] is the moisture storage capacity of the porous material, D_φ [kg.m⁻¹.s⁻¹] is the liquid conduction coefficient, δ_v [kg.m⁻¹.s⁻¹.Pa⁻¹] is the water vapor permeability of the porous material, φ [%] is the relative humidity, p_{sat} [Pa] is the water vapor saturation pressure, and $\frac{dH}{dT} = C$ [J.m⁻³.K⁻¹] is the heat storage capacity of the porous material.

This model belongs to Fraunhofer Institut Für BauphysiK IBP. It was then integrated into the WUFI (Wärme Und Feuchte Instationär) software package, one of the most widely used commercial tools for modeling heat and moisture transfer. This software is used to model the hygrothermal behavior of multilayered building elements exposed to the natural climate. This model has been used by several researchers [59–64], with generally satisfactory results.

As shown by many authors, it is possible to explicitly present the temperature by modifying the saturation pressure term as it can be expressed as a function of temperature. The novel system of coupled heat and mass transfer equation becomes [65–70]:

$$\frac{dw}{d\varphi} \frac{d\varphi}{dt} = \nabla \left(D_w^\varphi \nabla \varphi + D_w^T \nabla T \right) \quad (41)$$

$$\frac{dH}{dT} \frac{dT}{dt} + \frac{dH}{d\varphi} \frac{d\varphi}{dt} = \nabla \left(D_e^T \nabla T + D_e^\varphi \nabla \varphi \right) \quad (42)$$

where D_e^T [W.m⁻¹.K⁻¹], D_e^φ [W.m⁻¹], D_w^T [kg.m⁻¹.s⁻¹], and D_w^φ [kg.m⁻¹.s⁻¹.K⁻¹] are the material specific transport coefficients defined by the following expressions:

$$D_e^T = \lambda + (h_v + C_{p,v}T)\delta_v \cdot \varphi \frac{dp_{sat}}{dT} \quad (43)$$

$$D_e^\varphi = (h_v + C_{p,v}T)p_{sat} \cdot \delta_v \quad (44)$$

$$D_w^T = \varphi \cdot \delta_v \frac{dp_{sat}}{dT} \quad (45)$$

$$D_w^\varphi = p_{sat} \delta_v + K^* \quad (46)$$

A more detailed model has been proposed with additional terms on the material specific transport coefficient [71,72] and a source term to the mass transfer equation. The new system of equations becomes:

$$\frac{dw}{d\varphi} \frac{d\varphi}{dt} = \Delta \left(\left(\delta_v p_{sat} + K_l \rho_l R_D \frac{T}{\varphi} \right) \nabla \varphi + \left(\varphi \cdot \delta_v \frac{dp_{sat}}{dT} + K_l \rho_l r_v \ln(\varphi) \right) \nabla T \right) - \nabla \left(j_a \frac{0.622}{p_{atm}} \varphi p_{sat} \right) \quad (47)$$

$$\frac{dH}{dT} \frac{dT}{dt} = \Delta \left(D_e^T \nabla \varphi + D_e^\varphi \nabla \varphi \right) - \nabla \left(C_{p,a} j_a T + \frac{0.622}{p_{atm}} j_a h_v \varphi p_{sat} \right) \quad (48)$$

where K_l [kg.m⁻¹.s⁻¹.Pa⁻¹] is liquid water permeability, p_{atm} [Pa] is atmospheric pressure, and $C_{p,a}$ [J.kg⁻¹.K⁻¹] is the air heat capacity.

Wang et al. [73] developed a transient model for the coupled heat and moisture transfer in building materials based on the PCC introduced by Luikov. The temperature and relative humidity were used as the driving potentials. At the exception of the other PCC-based models, the PCC was introduced in both the energy conservation equation and the moisture conservation equation to simplify the model not only in the energy conservation equation.

$$(1 - \varepsilon) C_m \frac{\partial \varphi}{\partial t} = \nabla \left(D_{\varphi,l} \nabla \varphi \right) \quad (49)$$

$$\left(\rho_s C_{p,s} + w C_{p,l} \right) \frac{\partial T}{\partial t} = \nabla (\lambda \nabla T) + C_m (\varepsilon h_{lv} + \gamma) \frac{\partial \varphi}{\partial t} \quad (50)$$

The expression of the PCC in isothermal and non-isothermal conditions is as follows:

$$\varepsilon = \frac{D_{m,v}}{D_m} = \frac{\delta_v p_v}{K_l \rho_l r_v T + \delta_v p_v} \tag{51}$$

$$\varepsilon = \frac{|\delta_v \varphi \frac{dp_s}{dT} \nabla T + \delta_v p_s \nabla \varphi|}{|\delta_v \varphi \frac{dp_s}{dT} \nabla T + \delta_v p_s \nabla \varphi| + |K_l \rho_l r_v \ln \varphi \nabla T + K_l \rho_l r_v \frac{T}{\varphi} \nabla \varphi|} \tag{52}$$

3.2.3. Models Using Capillary Pressure as Driving Potential

Moisture transfer is often considered to be driven by capillary pressure gradients, as this quantity is an actual potential [74,75]. Capillary pressure p_c [pa] is defined as the pressure difference between the liquid and gas phases:

$$p_c = p_l - p_{v+a} \tag{53}$$

Janssen et al. [76] proposed a numerical model for simulations of moisture and heat transfer in building components under atmospheric excitation based on the model. Temperature and capillary pressure are used as driving potentials. The set of heat and mass transfer equations are:

$$\frac{\partial w}{\partial p_c} \frac{\partial p_c}{\partial t} = -\nabla(j_{m,l} + j_{m,v}) \tag{54}$$

$$\left(\rho_s C_{p,s} + w C_{p,l}\right) \frac{\partial T}{\partial t} + \left(C_{p,l} T \frac{\partial w}{\partial p_c}\right) \frac{\partial p_c}{\partial t} = \nabla(j_{h,c} + j_{h,a}) \tag{55}$$

$$j_{m,l} = -K_l \nabla p_c \tag{56}$$

$$j_{m,v} = -\frac{\delta_v p_v}{\rho_l r_v T} \nabla p_c - \frac{\delta_v p_v}{\rho_l r_v T^2} (\rho_l h_{lv} + p_c (T\gamma - 1)) \nabla T \tag{57}$$

$$j_{h,c} = -\lambda \nabla T \tag{58}$$

$$j_{h,a} = C_{p,l} T j_l + (C_{p,v} T + h_{lv}) j_v \tag{59}$$

Li et al. [77] also used capillary pressure as driven potential for the moisture transfer and temperature gradient for the heat transfer. The governing equations for the heat, air, and moisture transport in building materials are based on conservation of the combined heat and moisture transport of the representative elementary volume and expressed in the coefficient term as:

$$d_a \begin{bmatrix} \frac{\partial T}{\partial t} \\ \frac{\partial p_c}{\partial t} \end{bmatrix} = \nabla \left(b \nabla \begin{bmatrix} T \\ p_c \end{bmatrix} \right) + \varepsilon \nabla \begin{bmatrix} T \\ p_c \end{bmatrix} + \begin{bmatrix} Q_h \\ Q_m \end{bmatrix} \tag{60}$$

d_a is the damping coefficient matrix and written as:

$$d_a = \begin{bmatrix} \left(\rho_s C_{p,s} + w C_{p,l}\right) & 0 \\ 0 & \left(\frac{\partial w}{\partial p_c}\right) \end{bmatrix} \tag{61}$$

b is the diffusive coefficient matrix and written as:

$$b = \begin{bmatrix} \left(\lambda + \delta_v h_{lv} \varphi \frac{dp_s}{dT}\right) & \left(-\frac{\delta_v h_{lv} \varphi p_s}{\rho_l R_v T}\right) \\ \left(-\delta_v \varphi \frac{dp_s}{dT}\right) & \left(k_l + \frac{\delta_v \varphi p_s}{\rho_l R_v T}\right) \end{bmatrix} \tag{62}$$

ε is the convective coefficient matrix and written as:

$$\varepsilon = v \left[\begin{array}{c} \left(-\left(\rho_a C_{p,a} + h_{lv} \left(\frac{d\rho_v}{dT} \right) \right) \right) \left(\begin{array}{c} \left(\frac{h_{lv} \varphi}{\rho_l R_v T} \right) \left(\frac{d\rho_v}{d\varphi} \right) \\ \left(\frac{d\rho_v}{dT} \right) \end{array} \right) \\ \left(\frac{d\rho_v}{dT} \right) \end{array} \right] \quad (63)$$

The model is validated through intermodel comparisons with benchmarking cases of the HAMSTAD project and with experimental results of full-scale wall panels.

Fang et al. [78,79] developed a model similar to the model of Li et al. with capillary pressure and temperature as driven potential. The validation of the model was accomplished by comparing the simulation results with the experiment results in the study of Odgaard et al. [80].

3.2.4. Models Using Pressure Vapor as Driving Potential

Berger et al. [82] developed a detailed mathematical model combined with an innovative efficient numerical model to predict heat, air, and moisture transfer through porous building materials. The model is based on Luikov's work and uses the Whitaker volume averaging method to link the microscopic and macroscopic approaches. The model considers the transient effects of air transport and its impact on the heat and moisture transfer. Temperature, partial vapor pressure, and total pressure are used as driving potentials. The system of coupled heat, air, and mass transfer differential equations is as follows:

$$c_m \frac{\partial p_v}{\partial t} = \nabla (k_m \nabla p_v - a_v p_v) \quad (64)$$

$$C_q \frac{\partial T}{\partial t} = \nabla (k_q \nabla T + a_q T) + h_v \nabla (\delta_v \nabla p_v - a_v p_v) - \sum_{i=1}^3 \nabla (c_i T) j_{c,i} - C_{p,v} h_v \frac{\partial p}{\partial t} + C_{p,s} h_v \frac{\partial \sigma}{\partial t} \quad (65)$$

$$C_a \frac{\partial p}{\partial t} = \nabla (\delta_a \nabla p) - \nabla (\delta_v \nabla p_v - a_v p_v) + C_{av} \frac{\partial p_v}{\partial t} + C_{at} \frac{\partial T}{\partial t} + C_{as} \frac{\partial \sigma}{\partial t} \quad (66)$$

where a_v [s.m^{-1}] and a_q [$\text{W.m}^{-2}.\text{K}^{-1}$] are the advection coefficients, and C_q [$\text{J.m}^{-3}.\text{K}^{-1}$], c_m [$\text{Kg.m}^{-3}.\text{Pa}^{-1}$], C_a [Kg.J^{-1}], C_{as} [Kg.Pa.J^{-1}], C_{av} [Kg.J^{-1}], C_{at} [$\text{Kg.Pa.J}^{-1}.\text{K}^{-1}$], C_{qv} [Kg.J^{-1}], and C_{qs} [Kg.Pa.J^{-1}] the storage coefficients.

Ayres de Mello et al. [83,84] proposed a new mathematical model called CAR-HAM (Conductive, Advective, and Radiative Heat, Air, and Moisture) that includes the radiative transfer equation to calculate the thermal radiation effects within the porous materials to be taken into account in the energy balance. The formulation is based on the model presented in the HAMSTAD (heat, air, and moisture standard development) project, adding the contribution related to radiation. The moisture and the energy conservation equations are simultaneously solved using a fully implicit scheme and the MTDMA (MultiTridiagonal-MatrixAlgorithm) algorithm. The system of moisture and energy balance equations including the radiation contribution is presented as follows:

$$\frac{\partial w}{\partial t} = -\nabla j_{tot} \quad (67)$$

$$j_{tot} = j_v + j_l \quad (68)$$

$$j_v = -\delta_v \nabla p_v + u \rho_v \quad (69)$$

$$j_l = -k_l (\nabla p_{suc} - \rho_l g) \quad (70)$$

$$\frac{\partial H}{\partial t} = -\nabla j_q \quad (71)$$

$$j_{tot} = \lambda \nabla T + u \rho_c c_a T + j_v h_{lv} + j_l c_l T + q_{rad} \quad (72)$$

The radiative flux is calculated using Equation (73):

$$\nabla q_{rad} = \kappa \left(4\pi I_b - \int_0^{4\pi} I d\Omega \right) \quad (73)$$

3.3. Co-Simulation Approach

The building simulation programs such as TRNSYS and EnergyPlus do not accurately include hygrothermal interactions with the building envelope. Therefore, it is essential to integrate a non-isothermal combined heat and mass transfer model into the simulation environment. To overcome this problem and better stimulate the hygrothermal behavior of buildings, several approaches have been proposed in recent years. One of these is co-simulation, which consists in using two existing software packages, one for dynamic building simulation, and the other for precise modeling of hygrothermal behavior at the envelope level.

Zhai et al. [88] classified the co-simulation methods in two groups as either static or dynamic coupling. In static coupling, the interaction between the two simulation tools is one-way, with information flowing from one software program to the other without any feedback or iterative exchange during the simulation. On the other hand, dynamic coupling involves a two-way interaction between the tools, allowing a continuous exchange of information and feedback during the simulation process. Dynamic coupling enables a more comprehensive and accurate representation of the hygrothermal behavior of buildings, as it accounts for the mutual influence of heat and moisture transfer phenomena, leading to improved predictions and a better understanding of the building's performance.

In order to investigate the effects of sorption isotherm hysteresis on indoor climate and energy demand, Kwiatkowski et al. [89] developed and implemented in the energy performance simulation tool TRNSYS a new module for precise representation of mass transfer in materials in contact with indoor air, which is called Humi-mur.

Steeman et al. [57,58] developed a coupled TRNSYS-HAM model that can account for the response of a multizone building on moisture buffering effects in a more detailed way. The HAM model describes one dimensional transient coupled heat and mass transfer in porous materials. To illustrate the applicability of the integrated TRNSYS-HAM model for the design and evaluation of numerous building applications, the model was used to predict the surface relative humidity in an office space equipped with a gypsum cooled ceiling. Results show that a simplified model overpredicts the surface relative humidity because non-isothermal vapor diffusion in the hygroscopic gypsum layer is neglected.

Ferroukhi et al. [90–92] have extended their work by developing a co-simulation platform HAM-BES (BES: Building Energy Simulation) in order to accurately predict the hygrothermal behavior of the wall and living environment in buildings. This has enabled researchers to highlight the impact of hygrothermal transfer on the prediction of energy consumption and to study the effectiveness of different ventilation methods (extraction or insufflation) in controlling and reducing the risk of disorders caused by humidity.

Frasca et al. [93] proposed a multi-step methodology to investigate the capability of BES software coupled with a HAM model (HAM-BES) as a technique for diagnostics and conservation in complex settings. The methodology was thus applied to the historic church of the 17th century Chiesa di Santa Rosalia (Italy), allowing for the exploration of climate-induced conservation risks based on simulations.

3.4. Boundary Condition

In addition to the physical modeling of heat and moisture transfer coupled equations, boundary conditions such as ambient conditions and climatic data are necessary for accurate simulations and assessments. The boundary conditions are classified as interior and exterior conditions and expressed simultaneously for heat and moisture transfer.

The outside boundary condition is governed by several parameters, including the ambient air temperature, the relative humidity, solar radiation, and rain load. The outer and inner surface boundary conditions are given by [21,43,94]:

$$j_{v,ext} = \beta_{m,ext} (p_{v,ext} - p_{v,surf,ext}) \quad (74)$$

$$j_{q,ext} = h_{c,ext} (T_{ext} - T_{surf,ext}) + h_{lv} j_{v,ext} + \alpha q_{solar} \quad (75)$$

$$j_{m,int} = \beta_{m,int} (p_{v,int} - p_{v,surf,int}) \quad (76)$$

$$j_{q,int} = h_{c,int} (T_{air,int} - T_{surf,int}) + h_{lv} j_{v,int} \quad (77)$$

It should be noticed that liquid flux is not considered in both interior and exterior surfaces. In fact, it is reasonable to assume that there is no liquid water penetrating the indoor boundary surface (interior surface of the wall). This is because the interior of a building is generally designed to be dry, and measures are taken to prevent water intrusion from the outside. In the absence of wind-driven rain, the same assumption holds true for the outer boundary surface. However, when wind-driven rain is present, it can lead to rainwater accumulation on the exterior wall, ultimately resulting in surface saturation [76,95,96].

3.5. Models Validation

The validation of hygrothermal simulation models can be done in various ways. To make sure that model errors are not hidden by any uncertainties of input data or test results, a rigorous validation should comprise three steps. The first step is the confirmation of correct implementation of physical fundamentals by comparison with analytical solutions when it is possible. For moisture uptake in a semi-infinite region, there is a benchmark example in BS EN 15026:2001 [97]. As the second step, it is useful to compare the calculation results to laboratory tests with well-defined boundary conditions and material data. The third step should be close to the real thing, e.g., simulating the transient hygrothermal behavior of a building envelope component exposed to the natural climate.

Dong et al. [21] and Judkoff et al. [98] highlighted three commonly used methods for model validation: theoretical, intermodel, and experimental validation. A summary of the model validation methods is presented in Table 2.

Table 2. Summary of the model validation methods.

Validation Methods		References
Theoretical validation		[56,73,75,99–104]
Intermodel validation		[99,105–112]
Experimental validation	Material scale	[16,17,21,68,113–118]
	Wall scale	[2,94,119–126]

3.5.1. Theoretical Validation

In the theoretical validation, the model's predictions are compared with analytical solutions or well-established theoretical equations. HAMSTAD Benchmark case #2 [75] is an efficient theoretical validation case study for moisture transfer models. It describes the moisture redistribution in a homogeneous single-layer wall under isothermal conditions. Since the temperature difference through the interior and exterior of the wall is eliminated, an analytical solution can be obtained. Several authors has used this analytical method to validate their modeling [73,99–102]. In addition to the Benchmark, some authors developed analytical tools to solve heat and mass transfer problems [56,103,104]. Qin et al. [56] proposed an analytical method to calculate the coupled heat and moisture transfer process in building materials based on Laplace transformation and the Transfer Function Method. The transient temperature and moisture content distribution across the material can thus be

easily obtained from the solutions. The results were compared with the experimental data and other analytical solutions available in the literature; a good agreement was obtained.

3.5.2. Intermodel Validation

The intermodel validation method involves comparing the results of the model in question with those obtained from other independently developed models that aim to simulate similar phenomena. By comparing the outcomes, researchers can assess the consistency and accuracy of the model's predictions against other established models. This method can be divided into two categories: comparison with the numerical results of previous research literature and comparison with the simulated results of hygrothermal simulation software, such as COMSOL Multiphysics [99,105,106], WUFI [107–110], and Delphin [111,112]. In addition, the HAMSTAD Benchmark cases #3–5 [98] are often used for intermodel validation for numerous models.

3.5.3. Experimental Validation

In the experimental validation method, the model's predictions are compared with real-world experimental data obtained from physical tests or measurements. This approach is crucial as it enables researchers to verify how well the model replicates the actual behavior observed in experiments.

Busser et al. [20] reviewed the recent experimental studies to validate the hygrothermal models for building materials and envelopes and divided the experimental facilities into two scales: material and wall. At the material scale, two types of experimental facilities were distinguished: the climatic chamber [16,17,21,68,113–115] and the wind air tunnel [116–118]. These facilities differ only in the way convective boundary conditions were controlled. The wall scale can be divided into exposure to controlled conditions in the climate chamber (including one-sided and doubled-sided responses) [93,118–122] or natural outdoor conditions on one side (including single-layer and multilayer walls) [2,124–126].

4. Integration of Phase Change Materials in HAM Models

4.1. Modeling of PCMs

Solid–liquid phase change is generally described by the classic Stefan problem, named after the Slovenian physicist Joseph Stefan, who studied the solidification of soil and the formation of ice in the oceans around 1890 [127]. The Stefan problem describes the evolution of the boundary between two phases of a material undergoing a process of phase change. This problem is treated by solving the heat equations in the two regions (solid and liquid) with associated initial and boundary conditions. The temperature at the solid–liquid interface is the phase-change temperature. As the equations for the two phases are not valid at the interface, also known as the melting or solidification front, a final equation is introduced to close the mathematical system: the Stefan condition. This condition is obtained by performing an energy balance, which makes it possible to determine the position of the phase-change front:

Solid phase:

$$\rho C_{p,sol} \frac{\partial T_{sol}}{\partial t} = \frac{\partial}{\partial x} \left(\lambda_{sol} \frac{\partial T_{sol}}{\partial x} \right) \quad (78)$$

Liquid phase:

$$\rho C_{p,liq} \frac{\partial T_{liq}}{\partial t} = \frac{\partial}{\partial x} \left(\lambda_{liq} \frac{\partial T_{liq}}{\partial x} \right) \quad (79)$$

Stefan's condition for energy conservation at the boundary:

$$\frac{\partial}{\partial x} \left(\lambda_{sol} \frac{\partial T_{sol}}{\partial x} \right) - \frac{\partial}{\partial x} \left(\lambda_{liq} \frac{\partial T_{liq}}{\partial x} \right) = \rho L_f v \quad (80)$$

Under certain assumptions such as steady state, constant properties, and one-dimensionality, it is possible to solve Stefan's problem analytically. However, numerical methods are gen-

erally used to solve this system of equations when more realistic and complex scenarios are considered. These numerical methods can be divided into three groups [35]: fixed-grid methods, interface tracking methods, and hybrid methods.

In fixed-domain methods, Stefan's condition is taken into account implicitly by reformulating the conservation equations, and the position of the boundary is known a posteriori, i.e., once the solution has converged. Fixed-domain methods are characterized by their ease of implementation, convenience, adaptability, and versatility compared with other methods [128]. Latent heat can be taken into account using the enthalpy method, the apparent heat capacity method, the temperature transformation model, and the heat source method. Al-Saadi and Zhai [34] have carried out a review of all these methods, the synthesis of which will be presented in this section.

4.1.1. The Enthalpy Method

The enthalpy method was proposed by Eyres [129] to deal with thermal properties whose evolution depends on temperature. In this method, the sensible and latent heat terms are combined into an enthalpy term in the energy conservation equation. For heat transfers governed mainly by conduction, the conservation equation is described by Equation (81).

$$\rho \frac{\partial h(T)}{\partial t} = \frac{\partial}{\partial x} \left(\lambda \frac{\partial T}{\partial x} \right) \quad (81)$$

The enthalpy term represents the sum of two contributions: a sensible part (liquid and solid) and a latent part, whose respective expressions are described in Equations (79)–(81):

$$h(T) = h_{sensible}(T) + h_{latent}(T) \quad (82)$$

$$h_{sensible}(T) = \int_{T_{intiale}}^{T_{fusion}} C_{p,sol}(T) dT + \int_{T_{fusion}}^{T_{fusion}} C_{p,liq}(T) dT \quad (83)$$

$$h_{latent}(T) = f(T) L_f \quad (84)$$

where L_f [J.kg⁻¹] is the latent heat of fusion and $f(T)$ the liquid fraction as function of temperature.

The variation of enthalpy as a function of H-T temperature is obtained experimentally by calorimetry or by integrating the apparent heat capacity curve obtained by differential scanning calorimetry (DSC), which improves the accuracy of simulations.

This equation is nonlinear in the sense that enthalpy and thermal conductivity are temperature-dependent. It can be solved either using a nonlinear solver (Newton's method) or by linearizing the equation.

The enthalpy method has a number of advantages: (i) it is valid over a wide range of cases, from isothermal phase change to phase change over a temperature range, (ii) it is independent of the discretization scheme chosen (Finite Volume, Finite Difference, Finite Elements), (iii) no conditions have to be imposed on the change front, which is automatically taken into account [35]. The method is also simple, and the agreement with experimental data is good, making it one of the most widely used methods for modeling solidification/melting problems.

However, this method still faces two problems: it is difficult to take into account undercooling problems, and the temperature in a mesh can oscillate over time [130,131].

4.1.2. The Heat Capacity Method

In this method, the heat capacity is modified around the phase-change temperature to include latent heat. Two approaches are proposed in the literature to take this latent heat into account: the apparent heat capacity method and the effective heat capacity method. These two methods differ only in the approximation made to the heat capacity.

The apparent heat capacity method was introduced by Hashemi and Spielcevic [132] to solve a heat transfer problem with a phase change. The unsteady one-way conduction equation can be rewritten using the apparent heat capacity method as follows:

$$\rho C^{app}(T) \frac{\partial T}{\partial t} = \frac{\partial}{\partial x} \left(\lambda \frac{\partial T}{\partial x} \right) \quad (85)$$

where $C^{app}(T)$ represents the apparent heat capacity, which can be calculated in two different ways: either using analytical/experimental relationships or using numerical approximations.

Analytical/experimental relationships are obtained using thermo-physical characterization techniques such as DSC or the T-history method [133]. These characterization techniques provide material properties such as melting temperature, enthalpy of phase change, and heat capacities of the liquid and solid phases. These data are used to estimate the heat capacity of PCM using a simple direct relationship by introducing a fictitious phase change range (2ϵ):

$$C^{app} = \begin{cases} C_{p,sol} & \text{if } T < T_f - \epsilon \\ \frac{C_{p,sol} + C_{p,liq}}{2} + \frac{L_f}{2\epsilon} & \text{if } T_f - \epsilon \leq T \leq T_f + \epsilon \\ C_{p,sol} & \text{if } T > T_f + \epsilon \end{cases} \quad (86)$$

The choice of phase change range is a very important parameter when modeling with the apparent heat capacity method, as it can lead to convergence problems. If the range is too small or the time step too large, there is a risk of missing the latent heat contribution. It is therefore essential to carry out a parameter study to estimate the optimum values for these parameters.

Moreover, the accuracy of the method depends on the approximation made to the apparent heat capacity curve used in the simulation. Several shapes are proposed in the literature: rectangular, triangular, Gaussian, trapezoidal. Triangular and Gaussian profiles give better results than the other two [34].

To solve the convergence problem associated with analytical/experimental relationships, some authors have proposed an approach based on a numerical approximation of the heat capacity. Thus, Comini [134] expressed the heat capacity as a temperature derivative of enthalpy in a numerical resolution using the finite element method. Morgan et al. [135] improved this method by using an iterative scheme in which the heat capacity is approximated using successive temperature and enthalpy solutions.

$$C^{app} = \frac{\Delta h}{\Delta T} = \frac{h^n - h^{n-1}}{T^n - T^{n-1}} \quad (87)$$

Another alternative is to use the effective heat capacity method proposed by Poirier et al. [136]. In this method, a temperature profile is considered between nodes and instead of calculating the apparent heat capacity from the nodal point temperature, an effective heat capacity is calculated by integrating heat capacity across the nodal volume and the assumed temperature profile as follows:

$$C_{eff} = \frac{[\int C_a dV]}{V} \quad (88)$$

Despite being more accurate than the apparent heat capacity method, this method faces the same problems as the latter, due to the discontinuity around the phase change. This problem arises mainly for materials with isothermal phase change, where temperature jumps around the change are avoided, and materials with phase change, where latent heat is not taken into account.

Although this method is more efficient than the apparent heat capacity method, its calculation and implementation costs are higher.

4.1.3. The Heat Source or Enthalpy-Porosity Method

In the heat source or enthalpy-porosity method, the enthalpy term is divided into sensible and latent heat, which is considered a heat source. The energy conservation equation thus deviates:

$$\rho C_{avg}(T) \frac{\partial T}{\partial t} = \frac{\partial}{\partial x} \left(\lambda \frac{\partial T}{\partial x} \right) - \rho L_f \frac{\partial f}{\partial t} \quad (89)$$

The phase change front is known by evaluating the liquid fraction field at each node. The value of the liquid fraction is 0 for the solid phase, 1 for the liquid phase, and varies between]0 ;1[for the phase change range. It is generally approximated by the linear auxiliary function shown in the equation, where $T_{solidus}$ is the highest temperature at which the material is completely solid and $T_{liquidus}$ the lowest temperature at which the material is completely liquid:

$$f(T) = \begin{cases} 0 & \text{if } T < T_{solidus} \\ \frac{T - T_{solidus}}{T_{liquidus} - T_{solidus}} & \text{if } T_{solidus} \leq T \leq T_{liquidus} \\ 1 & \text{if } T > T_{liquidus} \end{cases} \quad (90)$$

Material properties are thus written as a function of the liquid fraction to consider the transition between the two phases:

$$C_{avg} = (1 - f(T))C_{p,sol}(T) + f(T)C_{p,liq}(T) \quad (91)$$

$$\lambda = (1 - f(T))\lambda_{sol}(T) + f(T)\lambda_{liq}(T) \quad (92)$$

$$\rho = (1 - f(T))\rho_{sol}(T) + f(T)\rho_{liq}(T) \quad (93)$$

The enthalpy porosity method is very intuitive, converges quickly with good accuracy, and is widely used when convection plays a very important role. One of the constraints of this method is its dependence on the mesh size. Indeed, depending on the mesh size chosen, numerical diffusion may occur at the solid–liquid interface. This problem can be solved by coupling the method with advanced numerical techniques such as adaptive meshing.

4.1.4. Phase-Field Model

The phase-field model, mainly used to study crystal growth during solidification, consists in using an auxiliary field to characterize the phase of the medium as a function of position and time. The transition between the different phases is tracked using the values of the phase parameter, enabling, in a similar way to the enthalpy model, an intermediate zone between the different phases. The equation for the evolution of the phase parameter for a pure material is described by Equation (94), and its value is between -1 and 1 [137]. It is possible to write a modified heat transfer equation as a function of the parameter.

$$\alpha \varepsilon^2 \frac{\partial \phi}{\partial t} = \varepsilon^2 \frac{d^2 \phi}{dx^2} - \frac{1}{2} (\phi^3 - \phi) + \frac{\varepsilon s}{2\sigma} (T - T_f) (1 - \phi^2) \quad (94)$$

α is the relaxation scale coefficient, σ [$\text{J} \cdot \text{m}^{-2}$] is the surface tension, s [$\text{J} \cdot \text{m}^{-3} \cdot \text{K}^{-1}$] is the entropic density difference between the phases, and ε [m] is the thickness of the solid–liquid interface.

$$\alpha \rho C_p \frac{\partial T}{\partial t} = \frac{\partial}{\partial x} \left(\lambda \frac{\partial T}{\partial x} \right) - \frac{1}{2} \rho L_f \frac{\partial \phi}{\partial t} \quad (95)$$

The relationship between the phase parameter and the liquid fraction gives the following system of equations:

$$\begin{cases} \rho C_p \frac{\partial T}{\partial t} = \frac{\partial}{\partial x} \left(\lambda \frac{\partial T}{\partial x} \right) - \rho L_f \frac{\partial f}{\partial t} \\ \frac{\partial f}{\partial t} = \frac{s}{\alpha \varepsilon \sigma} (T - T_f) f(1 - f) \end{cases} \quad (96)$$

This method has gained considerable popularity in the modeling of phase transformation and multiphase flow due to its ability to directly incorporate phase transition thermodynamics into the formulation [138].

A summary of the advantages and disadvantages of the different PCM models is presented in Table 3.

Table 3. Summary of the advantages and disadvantages of the different PCM models.

Models	Advantages	Disadvantages
Enthalpy	<ul style="list-style-type: none"> - Fast - Simple and accurate - Deals with sharp as well as gradual phase change 	<ul style="list-style-type: none"> - Difficulty to handle supercooling - Oscillation of temperature in a grid over time
Heat capacity	<ul style="list-style-type: none"> - Easy to implement - Suitable for gradual phase change - Temperature as only variable 	<ul style="list-style-type: none"> - Sensitive to the phase change range - accuracy of the method depends on the approximation made to the apparent heat capacity curve - Not applicable for cases where phase change occurs at fixed temperature
Heat source	<ul style="list-style-type: none"> - Very intuitive - Converges quickly - Good accuracy 	<ul style="list-style-type: none"> - Dependence on the mesh size creating numerical diffusion may occur at the solid–liquid interface
Phase-field	<ul style="list-style-type: none"> - Ability to incorporate phase transition thermodynamics - Highly robust and accurate method 	<ul style="list-style-type: none"> - Requires a precise discretization of the interface region - High computational cost

4.2. PCMs in HAM Models

PCMs can be incorporated into the entire building envelope: walls, roofs, windows, and floors [139–143]. Four experimental techniques for incorporating PCMs into building envelopes are presented in the literature: direct incorporation, impregnation, encapsulation, and shape-stabilized. Depending on the incorporation technique, different methods are used in the literature to numerically integrate PCMs in heat transfer models. Most of the studies in the literature concerned only the heat transfer aspect [144–149], and only few studies are reported on both heat and mass transfer aspects. Despite the literature being full of experimental characterization of the hygrothermal behavior of PCM composites, only few of these solutions are evaluated numerically. In this section, we propose to evaluate the different studies addressing the hygrothermal numerical behavior of building materials incorporating PCMs.

The first way is to consider the PCM as a different layer of the building envelope. Therefore, the whole building wall is modeled as a multilayer material with each layer defined by its set of characteristic equations. Fraire et al. [36] proposed a MPCM (micro-encapsulated PCM)/diatomite composite as an alternative solution for the substitution of EPS (expanded polystyrene) for adjusting indoor temperature and relative humidity. The MPCM/diatomite composite was modeled using the coupled heat and moisture transfer model of Kunzel et al. [25]. The PCM was incorporated into the porosity of the diatomite and modeled using a modified heat capacity method. The effective thermal properties of the media assuming a parallel configuration are:

$$(\rho C_p)_{eff} = \rho_d C_{pd} \theta_d + \rho_{PCM} C_{pPCM} (1 - \theta_d) \quad (97)$$

Comparable outcomes were observed by Shi et al. [150], where macro-encapsulated PCM was integrated into concrete walls. This integration demonstrated analogous effects in terms of enhancing temperature and humidity regulation.

Recently, Wu et al. [37] proposed a passive envelope solution that integrates a hydrocarbon-based PCM and hemp concrete to improve buildings' energy, thermal, and hydric performances simultaneously. The relative humidity and temperature are chosen as driving potentials of

moisture and heat transfer, respectively. The effective heat capacity model was chosen to describe the heat transfer of the PCM. Four integrated scenarios were considered and compared with a reference scenario (hemp concrete only). The performance of the integrated envelope was studied numerically based on the impact of the PCM's properties and its location in the envelope. As the PCM moves toward the interior, the energy and hygrothermal performances improve. Thus, it is recommended to place the PCM close to the interior as the total heat load, temperature amplitude, and partial water vapor pressure amplitude are reduced by 8.2%, 46.3%, and 43.7%, respectively, in summer and 1.3%, 9.1%, and 8.2%, respectively, in winter compared to the reference scenario.

Chang et al. [151] assessed the hygrothermal performance of building components, including wood-frame walls made of a macro-packed PCM (MPPCM) containing n-oc-tadecane, using the WUFI PRO 5.3 program. The results showed that the hygrothermal performance of the wood-frame structures applied to the MPPCM, which replaced the use of the vapor retarder, is improved. Also, the results of analysis of mold growth risk showed that it is possible to solve the problems of mold growth risk using MPPCM.

Zhu et al. [152] studied the effects of Phase Change Humidity Controlling Materials (PCHCM) wallboards on building energy consumption and indoor hygrothermal environment for the city of Wuhan in China, which has hot summers and cold winters. The PCM effect was integrated using the effective heat capacity method that allows the relationship between the specific heat capacity of dry materials and the temperature. The phase change temperature range was set to 1 °C, and Kunzel's model is used to describe the hygrothermal behavior. The simulation results based on TRNSYS showed that the PCHCM wallboard was able to both reduce energy consumption and improve indoor hygrothermal environment for the case study building significantly.

The second way is to model the PCM and hygrothermal material as a homogeneous material with unique properties. There are a few works reported in the literature using this method. A novel model for analyzing the hygrothermal performance of a PCHCM in a built environment is developed and validated using experimental data [153]. The model consists of a combined model of the heat and moisture transfer with the phase change process using the enthalpy method and Kunzel method. The numerical results indicate that PCHCM is suitable for the areas that simultaneously manifest a wide amplitude of hygrothermal (temperature and humidity) difference.

5. Assessment of Material Properties

The input parameters of each model including hygrothermal and phase change models are summarized in Table 4. These parameters are obtained from the experimental characterization of the material properties and can be classified as thermal and hydric properties. In the following, the techniques of characterization of each group of properties will be presented.

Table 4. Material hygrothermal properties and characterization techniques.

	Properties	Measurement Techniques
Hydric properties	Moisture content	- Gravimetric method: cup methods, DVS - Volumetric method
	Liquid permeability	- Direct methods - Inverse techniques
	Vapor permeability	Cup method
Thermal properties	Moisture storage capacity ($C_m = \frac{\partial w}{\partial \varphi}$)	Retrieve from the sorption isotherm
	Thermal conductivity (λ)	Hot plate method, guarded hotbox method, hot wire method, hot disk method, flash method
	Heat capacity (C_p)	
	Melting/fusion temperature	- DSC (dynamic and isothermal step method)
	Latent heat of fusion/crystallization	- T-history method

5.1. Hydric Properties

The sorption isotherm $w(\varphi)$ establishes how much water a material can either absorb or release based on the relative humidity of the surrounding environment while maintaining a constant temperature. Typically, the measurement of adsorption/desorption isotherms is carried out using two distinct methods: gravimetric methods and volumetric methods [154]. The principle involves regularly monitoring the change in the apparent mass of the studied material over time at various relative humidity levels. The humidity is controlled either by salt solutions (silica gel, magnesium nitrate, barium chloride) or by designed devices using water vapor such as Dynamic Vapor Sorption (DVA) and Vapor Sorption Analyzer (VSA). On the contrary, the volumetric methods consist of measuring the change in volume of water vapor adsorbed or released by the material. By placing a sample in a controlled volume, a specific amount of water vapor is injected until the targeted pressure is reached. Once equilibrium is achieved, the volume of vapor adsorbed by the material is determined. These approaches significantly reduce the testing time but involve working with small-sized samples combined with a dynamic flow of water vapor.

The moisture storage capacity is defined as the slope of the sorption isotherm curves ($C_m = \frac{\partial w}{\partial \varphi}$). The latter is an important input parameter for coupled heat, air, and moisture models. It represents the ability of the material to adsorb and release moisture when environmental moisture conditions change [8].

The general method to measure the liquid, vapor, or air diffusivities and permeabilities is to expose the material to a pressure gradient (vapor pressure, liquid pressure, or total pressure) and to measure the resulting flow. Each property has to be measured separately by avoiding the other pressure gradients or by making them negligible. As for the sorption isotherm, this method is a steady-state method.

In the case of vapor permeability (δ_v), the most commonly used measurement technique is the cup method, which adheres to the ISO 12572:2013 standard [155]. This method establishes a vapor pressure gradient by maintaining a difference in relative humidity between the two sides of the sample, while keeping the temperature constant. The change in mass is measured to determine the mass flow rate. The fundamental concept behind this method is to measure a consistent change in mass while controlling the flow of vapor, which is driven by the contrast in relative humidity between the two sides of the sample, all while maintaining a constant temperature.

Liquid water permeability (K_l) is a hygrothermal characteristic that describes the transfer of liquid water through porous materials and depends on the moisture content of the porous material. This property is assessed experimentally by measuring the liquid permeability at various moisture levels in the porous medium. Methods for determining this property can be classified into two categories: direct and inverse methods [156]. The

direct method consists of applying a liquid pressure gradient between the two ends of a sample to create a flow of liquid water through the porous material. The flow rate of the water passing through the sample is then measured. The values of the flow rate and the liquid pressure gradient are subsequently used in conjunction with Darcy's law to calculate the permeability. The principle of indirectly determining liquid permeability as a function of moisture content involves inducing the transfer of liquid water through a sample (typically through imbibition or drying) and measuring the change in relative humidity within the material. This test is then modeled within a hygrothermal transfer simulation tool, which calculates the evolution of relative humidity within the porous material. Permeability is then the optimized value that minimizes the difference between the simulated and measured relative humidities.

5.2. Thermal Properties

The thermal conductivity represents the ease with which heat spreads within a material based on a given temperature difference. It is one of the most important intrinsic properties of the hygrothermal behavior of a building. There are two types of measurement: steady state, where the medium is subjected to a flow that is independent of time (stationary), such as the guarded hot-plate method and the guarded hotbox method, and transient measurements such as the hot wire method, the hot disk method, the flash method, and the shock probe method [157]. These last two methods are the most widely used.

Specific heat C_p [$J \cdot K^{-1} \cdot g^{-1}$], also known as mass heat capacity or mass heat, defines the amount of energy required to raise one gram of material by one degree Celsius. This property can be measured by differential scanning calorimetry (DSC), a technique that measures the heat flux absorbed or released by the sample as a function of time for a specific temperature change in a controlled atmosphere. DSC is also used to measure the melting/solidification temperatures and enthalpies that are important properties for PCMs [158–161].

For some PCM models, it is important to know the shape of enthalpy–temperature curve with a temperature uncertainty $\delta T < 1$ K. The h-T curve is obtained using classical DSC under dynamic mode or isothermal step mode [133]. Due to its small sample size, DSC in general is not suitable for heterogeneous materials. For these PCMs, the T-history method can be used to determine h(T) data with sufficient precision. Other important properties used in numerical simulation of PCMs are the latent heat and temperature of fusion or solidification. These are essential input data used in all the PCM models described in Section 4.1. These properties are obtained also by using DSC. They can also be used to obtain the enthalpy function or the apparent heat capacity numerically.

6. Conclusions

The present study reviewed the hygrothermal models of PCMs integrated into building envelopes to evaluate the performance. First, the different models of HAM transfer in buildings are presented. These models have been divided into two groups: the nodal and HAM approaches.

Nodal models are suitable for steady-state analyses as well as quick assessments and are currently employed in the most common BES software, such as TRNSYS. They predominantly focus on simulating temperature variations and energy requirements in specific spaces on a larger scale. However, their moisture exchange models at the wall scale often rely on simplified approaches that do not consider the coupling of heat and moisture transfer phenomena through building envelopes. Two simplified models for surface moisture adsorption and desorption, namely the Effective Capacitance Moisture model and the Effective Moisture Penetration Depth model, are distinguished within the nodal framework.

Unlike the nodal approach, HAM models take into account the simultaneous movement of heat, air, and moisture within porous materials and offer a more comprehensive perspective on dynamic behavior and interactions. These models integrate various physical

processes such as conduction, convection, capillarity, and vapor diffusion. Several HAM approaches are presented in the literature. One of the key factors differentiating these models is the choice of transfer motors they take into account. Based on an extensive literature review, the different HAM models have been classified according to four driving potentials, which are relative humidity, vapor pressure, capillary pressure, and moisture content. The latter being discontinuous at the interface between two materials due to their different hygroscopic properties, it is not suitable for multilayer simulations. Several validation techniques exist for these models to test their accuracy, including theoretical, intermodel, and experimental validations.

Along with hygroscopic materials, PCMs has been identified as an efficient technique to increase the thermal capacity, energy efficiency, and comfort impact of buildings. There are several different approaches available for studying solid–liquid phase change. These include enthalpy-based methods, effective heat capacity methods, front tracking methods, and adaptive grid methods. The enthalpy-based and heat capacity methods are the most widely used in the literature.

Consequently, it is valuable to integrate the thermal inertia of PCMs with the moisture inertia of hygroscopic materials, making it possible to improve the energy, thermal, and hydric performance of the envelope simultaneously. However, when it comes to the integration of these two types of materials, most studies have focused only on their thermal and energy performance while neglecting their hydric performance. The literature lacks numerical methods to describe both phase change and hygroscopic behavior. It is therefore necessary to develop numerical models in order to fully assess the behavior of these hybrid materials capable of controlling both temperature and humidity. One potential modeling approach could involve employing a HAM model with pressure vapor and temperature as the driving potentials. The PCM's behavior could be effectively managed through an enthalpy-based method that allies simplicity and accuracy. These numerical models would be useful to conduct an optimization study prior to the material development in order to find the suitable materials properties for a specific application (weather conditions, for instance). This step is also essential to understand better the behavior of these hybrid materials and to assess their behavior in multiple scenarios.

Author Contributions: Conceptualization, all authors; methodology, all authors; formal analysis, all authors; investigation, all authors; resources, all authors; data curation, all authors; writing—original draft preparation, M.S.; writing—review and editing, all authors; visualization, all authors; supervision, R.B., M.D., A.E.A.H. and A.G.; project administration, R.B. and M.D.; funding acquisition, R.B. and M.D. All authors have read and agreed to the published version of the manuscript.

Funding: This work is carried out in the frame of Region Nouvelle Aquitaine for subsidizing BioMCP project (Project 2017-1R10209-13023) and in the frame of the Laboratory for Energy and Environmental Efficiency of Envelopes and Cities, 4ev Lab, the joint laboratory between EDF R&D, CNRS, LaSIE conducting research to improve the energy and environmental performance of buildings and the quality of life of the inhabitants of urban spaces.

Conflicts of Interest: The authors declare that they have no known competing financial interests or personal relationships that could have appeared to influence the work reported in this paper.

References

1. Liu, S.; Kwok, Y.-T.; Lau, K.; Ng, E. Applicability of Different Extreme Weather Datasets for Assessing Indoor Overheating Risks of Residential Buildings in a Subtropical High-Density City. *Build. Environ.* **2021**, *194*, 107711. [[CrossRef](#)]
2. Xia, D.; Zhong, Z.; Huang, Y.; Zou, Y.; Lou, S.; Zhan, Q.; Guo, J.; Yang, J.; Guo, T. Impact of Coupled Heat and Moisture Transfer on Indoor Comfort and Energy Demand for Residential Buildings in Hot-Humid Regions. *Energy Build.* **2023**, *288*, 113029. [[CrossRef](#)]
3. Hamard, E.; Cazacliu, B.; Razakamanantsoa, A.; Morel, J.C. Cob, a Vernacular Earth Construction Process in the Context of Modern Sustainable Building. *Build. Environ.* **2016**, *106*, 103–119. [[CrossRef](#)]
4. Niroumand, H.; Zain, M.F.M.; Jamil, M. Various Types of Earth Buildings. *Procedia Soc. Behav. Sci.* **2013**, *89*, 226–230. [[CrossRef](#)]
5. Evans, I.; Smiley, L.; Smith, M.G. *The Hand-Sculpted House: A Philosophical and Practical Guide to Building a Cob Cottage*; Chelsea Green Publishing: Chelsea, VT, USA, 2002.

6. Ben-Alon, L.; Loftness, V.; Harries, K.A.; Hameen, E.C.; Bridges, M. Integrating earthen building materials and methods into mainstream construction. *J. Green Build.* **2020**, *15*, 87–106. [[CrossRef](#)]
7. Watson, L.; McCabe, K. The Cob Building Technique. Past, Present and Future. *Inf. Constr.* **2011**, *63*, 59–70. [[CrossRef](#)]
8. Benmahiddine, F.; Cherif, R.; Bennai, F.; Belarbi, R.; Tahakourt, A.; Abahri, K. Effect of Flax Shives Content and Size on the Hygrothermal and Mechanical Properties of Flax Concrete. *Constr. Build. Mater.* **2020**, *262*, 120077. [[CrossRef](#)]
9. Delannoy, G.; Marceau, S.; Glé, P.; Gourlay, E.; Guéguen-Minerbe, M.; Diafi, D.; Nour, I.; Amziane, S.; Farcas, F. Aging of Hemp Shiv Used for Concrete. *Mater. Des.* **2018**, *160*, 752–762. [[CrossRef](#)]
10. Seng, B.; Lorente, S.; Magniont, C. Scale Analysis of Heat and Moisture Transfer through Bio-Based Materials—Application to Hemp Concrete. *Energy Build.* **2017**, *155*, 546–558. [[CrossRef](#)]
11. Abahri, K.; El Hachem, C.; Bennai, F.; Toan, N.; Belarbi, R. *Prediction of Hemp Concrete Morphological Deformation by X-Ray Tomography*; American Concrete Institute: Farmington Hills, MI, USA, 2017; Volume 320, pp. 616–625.
12. Recart, C.; Sturts Dossick, C. Hygrothermal Behavior of Post-Retrofit Housing: A Review of the Impacts of the Energy Efficiency Upgrade Strategies. *Energy Build.* **2022**, *262*, 112001. [[CrossRef](#)]
13. Wang, R.; Ge, H.; Baril, D. Moisture-Safe Attic Design in Extremely Cold Climate: Hygrothermal Simulations. *Build. Environ.* **2020**, *182*, 107166. [[CrossRef](#)]
14. Bastien, D.; Winther-Gaasvig, M. Influence of Driving Rain and Vapour Diffusion on the Hygrothermal Performance of a Hygroscopic and Permeable Building Envelope. *Energy* **2018**, *164*, 288–297. [[CrossRef](#)]
15. Liu, Y.; Wang, Y.; Wang, D.; Liu, J. Effect of Moisture Transfer on Internal Surface Temperature. *Energy Build.* **2013**, *60*, 83–91. [[CrossRef](#)]
16. Belarbi, R.; Qin, M.; Ait-Mokhtar, A.; Nilsson, L.-O. Experimental and Theoretical Investigation of Non-Isothermal Transfer in Hygroscopic Building Materials. *Build. Environ.* **2008**, *43*, 2154–2162. [[CrossRef](#)]
17. Qin, M.; Ait-Mokhtar, A.; Belarbi, R. Two-Dimensional Hygrothermal Transfer in Porous Building Materials. *Appl. Therm. Eng.* **2010**, *30*, 2555–2562. [[CrossRef](#)]
18. Bennai, F.; Ferroukhi, M.Y.; Benmahiddine, F.; Belarbi, R.; Nouviaire, A. Assessment of Hygrothermal Performance of Hemp Concrete Compared to Conventional Building Materials at Overall Building Scale. *Constr. Build. Mater.* **2022**, *316*, 126007. [[CrossRef](#)]
19. Trabelsi, A.; Belarbi, R.; Abahri, K.; Qin, M. Assessment of Temperature Gradient Effects on Moisture Transfer through Thermo-gradient Coefficient. *Build. Simul.* **2012**, *5*, 107–115. [[CrossRef](#)]
20. Busser, T.; Berger, J.; Piot, A.; Pailha, M.; Woloszyn, M. Comparison of Model Numerical Predictions of Heat and Moisture Transfer in Porous Media with Experimental Observations at Material and Wall Scales: An Analysis of Recent Trends. *Dry. Technol.* **2019**, *37*, 1363–1395. [[CrossRef](#)]
21. Dong, W.; Chen, Y.; Bao, Y.; Fang, A. A Validation of Dynamic Hygrothermal Model with Coupled Heat and Moisture Transfer in Porous Building Materials and Envelopes. *J. Build. Eng.* **2020**, *32*, 101484. [[CrossRef](#)]
22. Luikov, A.V. *Heat and Mass Transfer in Capillary-Porous Bodies*; Elsevier: Amsterdam, The Netherlands, 1966; pp. 233–303. ISBN 978-1-4832-0065-1.
23. Philip, J.R. Flow in Porous Media. *Annu. Rev. Fluid Mech.* **1970**, *2*, 177–204. [[CrossRef](#)]
24. Qin, M.; Belarbi, R.; Ait-Mokhtar, A.; Nilsson, L.-O. Coupled Heat and Moisture Transfer in Multi-Layer Building Materials. *Constr. Build. Mater.* **2009**, *23*, 967–975. [[CrossRef](#)]
25. Künzel, H. *Simultaneous Heat and Moisture Transport in Building Components. One- and Two-Dimensional Calculation Using Simple Parameters*; Fraunhofer IBP: Stuttgart, Germany, 1995.
26. Pedersen, C.R. Prediction of Moisture Transfer in Building Constructions. *Build. Environ.* **1992**, *27*, 387–397. [[CrossRef](#)]
27. Janssen, H.; Carmeliet, J.; Hens, H. The Influence of Soil Moisture in the Unsaturated Zone on the Heat Loss from Buildings via the Ground. *J. Therm. Envel. Build. Sci.* **2002**, *25*, 275–298. [[CrossRef](#)]
28. Basecq, V.; Michaux, G.; Blondeau, P.; Inard, C. Short Term Storage Systems of the Thermal Energy for Buildings: A Review. *Adv. Build. Energy Res.* **2013**, *7*, 66–119. [[CrossRef](#)]
29. Ben Romdhane, S.; Amamou, A.; Ben Khalifa, R.; Saïd, N.M.; Younsi, Z.; Jemni, A. A Review on Thermal Energy Storage Using Phase Change Materials in Passive Building Applications. *J. Build. Eng.* **2020**, *32*, 101563. [[CrossRef](#)]
30. Lamrani, B.; Johannes, K.; Kuznik, F. Phase Change Materials Integrated into Building Walls: An Updated Review. *Renew. Sustain. Energy Rev.* **2021**, *140*, 110751. [[CrossRef](#)]
31. Al-Rashed, A.A.A.A.; Alnaqi, A.A.; Alsarraf, J. Energy-Saving of Building Envelope Using Passive PCM Technique: A Case Study of Kuwait City Climate Conditions. *Sustain. Energy Technol. Assess.* **2021**, *46*, 101254. [[CrossRef](#)]
32. Bohórquez-Órdenes, J.; Tapia-Calderón, A.; Vasco, D.A.; Estuardo-Flores, O.; Haddad, A.N. Methodology to Reduce Cooling Energy Consumption by Incorporating PCM Envelopes: A Case Study of a Dwelling in Chile. *Build. Environ.* **2021**, *206*, 108373. [[CrossRef](#)]
33. Yang, Y.K.; Kang, I.S.; Chung, M.H.; Kim, S.; Park, J.C. Effect of PCM Cool Roof System on the Reduction in Urban Heat Island Phenomenon. *Build. Environ.* **2017**, *122*, 411–421. [[CrossRef](#)]
34. AL-Saadi, S.N.; Zhai, Z.J. Modeling Phase Change Materials Embedded in Building Enclosure: A Review. *Renew. Sustain. Energy Rev.* **2013**, *21*, 659–673. [[CrossRef](#)]

35. Zeneli, M.; Nikolopoulos, A.; Karellas, S.; Nikolopoulos, N. Chapter 7—Numerical Methods for Solid-Liquid Phase-Change Problems. In *Ultra-High Temperature Thermal Energy Storage, Transfer and Conversion*; Datas, A., Ed.; Woodhead Publishing Series in Energy; Woodhead Publishing: Sawston, UK, 2021; pp. 165–199. ISBN 978-0-12-819955-8.
36. Fraine, Y.; Seladji, C.; Aït-Mokhtar, A. Effect of Microencapsulation Phase Change Material and Diatomite Composite Filling on Hygrothermal Performance of Sintered Hollow Bricks. *Build. Environ.* **2019**, *154*, 145–154. [[CrossRef](#)]
37. Wu, D.; Rahim, M.; El Ganaoui, M.; Bennacer, R.; Liu, B. Multilayer Assembly of Phase Change Material and Bio-Based Concrete: A Passive Envelope to Improve the Energy and Hygrothermal Performance of Buildings. *Energy Convers. Manag.* **2022**, *257*, 115454. [[CrossRef](#)]
38. Crausse, P.; Laurent, J.P.; Perrin, B. Influence des phénomènes d’hystérésis sur les propriétés hydriques de matériaux poreux: Comparaison de deux modèles de simulation du comportement thermohydrique de parois de bâtiment. *Rev. Générale Therm.* **1996**, *35*, 95–106. [[CrossRef](#)]
39. Fick, A.V. On Liquid Diffusion. *Lond. Edinb. Phil. Mag.* **1855**, *10*, 30–39. [[CrossRef](#)]
40. Tariku, F.; Kumaran, K.; Fazio, P. Transient Model for Coupled Heat, Air and Moisture Transfer through Multilayered Porous Media. *Int. J. Heat Mass Transf.* **2010**, *53*, 3035–3044. [[CrossRef](#)]
41. Hens, H. Heat transfer. In *Building Physics—Heat, Air and Moisture: Fundamentals and Engineering Methods with Examples and Exercises*; Wiley: Hoboken, NJ, USA, 2017; pp. 15–124. [[CrossRef](#)]
42. Fourier, J.B.J. *Theorie Analytique de la Chaleur*; Didot: Paris, France, 1822; pp. 499–508.
43. Hamdaoui, M.-A.; Benzaama, M.-H.; El Mendili, Y.; Chateigner, D. A Review on Physical and Data-Driven Modeling of Buildings Hygrothermal Behavior: Models, Approaches and Simulation Tools. *Energy Build.* **2021**, *251*, 111343. [[CrossRef](#)]
44. Boyer, H.; Chabriat, J.P.; Grondin-Perez, B.; Tourrand, C.; Brau, J. Thermal Building Simulation and Computer Generation of Nodal Models. *Build. Environ.* **1996**, *31*, 207–214. [[CrossRef](#)]
45. TRNSYS. Transient System Simulation Tool. Available online: <https://www.trnsys.com/> (accessed on 8 August 2023).
46. Kerestecioglu, A.; Kamel, A. Theoretical and Computational Investigation of Simultaneous Heat and Moisture Transfer in Buildings: “Effective Penetration Depth” Theory. In Proceedings of the ASHRAE 1990 Winter Meeting, Atlanta, GA, USA, 11–14 February 1990.
47. Abadie, M.; Mendes, N. Comparative Analysis of Response-Factor and Finite-Volume Based Methods for Predicting Heat and Moisture Transfer through Porous Building Materials. *J. Build. Phys.* **2006**, *30*, 7–37. [[CrossRef](#)]
48. Luikov, A.V. Heat and Mass Transfer in Capillary-Porous Bodies. In *Advances in Heat Transfer*; Elsevier: Amsterdam, The Netherlands, 1964; Volume 1, pp. 123–184. ISBN 978-0-12-020001-6.
49. Irudayaraj, J.; Wu, Y. Analysis and Application of Luikov’s Heat, Mass, and Pressure Transfer Model to a Capillary Porous Media. *Dry. Technol.* **1996**, *14*, 803–824. [[CrossRef](#)]
50. Lewis, R.W.; Ferguson, W.J. The Effect of Temperature and Total Gas Pressure on the Moisture Content in a Capillary Porous Body. *Int. J. Numer. Methods Eng.* **1990**, *29*, 357–369. [[CrossRef](#)]
51. Mendes, N.; Ridley, I.; Lamberts, R.; Philippi, P.C.; Budag, K. Umidus: A PC program for the Prediction of Heat and Mass Transfer in Porous Building Elements. In Proceedings of the International Conference on Building Performance Simulation 99, Kyoto, Japan, 13–15 September 1999; pp. 277–283.
52. Mendes, N.; Philippi, P.C.; Lamberts, R. A New Mathematical Method to Solve Highly Coupled Equations of Heat and Mass Transfer in Porous Media. *Int. J. Heat Mass Transf.* **2002**, *45*, 509–518. [[CrossRef](#)]
53. Whitaker, S. Simultaneous Heat, Mass, and Momentum Transfer in Porous Media: A Theory of Drying. In *Advances in Heat Transfer*; Hartnett, J.P., Irvine, T.F., Eds.; Elsevier: Amsterdam, The Netherlands, 1977; Volume 13, pp. 119–203.
54. Milly, P.C.D. The Coupled Transport of Water and Heat in a Vertical Soil Column under Atmospheric Excitation. Master’s Thesis, Massachusetts Institute of Technology, Cambridge, MA, USA, 1980.
55. Abahri, K. Modélisation Des Transferts Couplés de Chaleur, d’air et d’humidité Dans Les Matériaux Poreux de Construction. Ph.D. Thesis, University of La Rochelle, La Rochelle, France, 2012.
56. Qin, M.; Belarbi, R.; Aït-Mokhtar, A.; Seigneurin, A. An Analytical Method to Calculate the Coupled Heat and Moisture Transfer in Building Materials. *Int. Commun. Heat Mass Transf.* **2006**, *33*, 39–48. [[CrossRef](#)]
57. Steeman, M.; Janssens, A.; Steeman, H.-J.; Van Belleghem, M.; De Paepe, M. On Coupling 1D Non-Isothermal Heat and Mass Transfer in Porous Materials with a Multizone Building Energy Simulation Model. *Build. Environ.* **2010**, *45*, 865–877. [[CrossRef](#)]
58. Steeman, M.; Van Belleghem, M.; De Paepe, M.; Janssens, A. Experimental Validation and Sensitivity Analysis of a Coupled BES–HAM Model. *Build. Environ.* **2010**, *45*, 2202–2217. [[CrossRef](#)]
59. Alioua, T.; Agoudjil, B.; Boudenne, A.; Benzarti, K. Sensitivity Analysis of Transient Heat and Moisture Transfer in a Bio-Based Date Palm Concrete Wall. *Build. Environ.* **2021**, *202*, 108019. [[CrossRef](#)]
60. Oumeziane, Y.A. Evaluation des performances hygrothermiques d’une paroi par simulation numérique: Application aux parois en béton de chanvre. Ph.D. Thesis, INSA de Rennes, Rennes, France, 2013.
61. Reuge, N.; Collet, F.; Pretot, S.; Moissette, S.; Bart, M.; Style, O.; Shea, A.; Lanos, C. Hygrothermal Effects and Moisture Kinetics in a Bio-Based Multi-Layered Wall: Experimental and Numerical Studies. *Constr. Build. Mater.* **2020**, *240*, 117928. [[CrossRef](#)]
62. Zirkelbach, D.; Mehra, S.-R.; Sedlbauer, K.-P.; Künzel, H.-M.; Stöckl, B. A Hygrothermal Green Roof Model to Simulate Moisture and Energy Performance of Building Components. *Energy Build.* **2017**, *145*, 79–91. [[CrossRef](#)]

63. Krejčí, T.; Kruis, J.; Šejnoha, M.; Koudelka, T. Numerical Analysis of Coupled Heat and Moisture Transport in Masonry. *Comput. Math. Appl.* **2017**, *74*, 229–248. [[CrossRef](#)]
64. Medjelekh, D.; Ulmet, L.; Gouny, F.; Fouchal, F.; Nait-Ali, B.; Maillard, P.; Dubois, F. Characterization of the Coupled Hygrothermal Behavior of Unfired Clay Masonries: Numerical and Experimental Aspects. *Build. Environ.* **2016**, *110*, 89–103. [[CrossRef](#)]
65. Nespoli, L.; Janetti, M.B.; Ochs, F. Comparing Different Approaches for Moisture Transfer inside Constructions with Air Gaps. In Proceedings of the COMSOL Conference, Rotterdam, The Netherlands, 23–25 October 2013; Volume 61.
66. Xu, Y.; Zeng, Z.; Sun, D. Experimental and Numerical Investigation on the Effect of Heat and Moisture Coupling Migration of Unsaturated Lateritic Clay for the Soil Thermal Storage System. *Energy Build.* **2022**, *276*, 112499. [[CrossRef](#)]
67. Promis, G.; Douzane, O.; Le, A.D.T.; Langlet, T. Moisture hysteresis influence on mass transfer through bio-based building materials in dynamic state. *Energy Build.* **2018**, *166*, 450–459. [[CrossRef](#)]
68. Thibaut, C.; Dylan, L.; Patrick, G. Hygrothermal behavior of bio-based building materials including hysteresis effects: Experimental and numerical analyses. *Energy Build.* **2014**, *84*, 617–627. [[CrossRef](#)]
69. Lelièvre, D. Simulation Numérique Des Transferts de Chaleur et d'humidité Dans Une Paroi Multicouche de Bâtiment En Matériaux Biosourcés. Ph.D. Thesis, Université de Bretagne Sud, Lorient, France, 2015.
70. Janetti, M.B.; Ochs, F.; Feist, W. 3D Simulation of Heat and Moisture Diffusion in Constructions. In Proceedings of the Comsol Conference Stuttgart 2011, Stuttgart, Germany, 26–28 October 2011.
71. Rong, L.; Yuewu, H. Heat and Moisture Transfer Characteristics of Multilayer Walls. *Energy Procedia* **2018**, *152*, 324–329. [[CrossRef](#)]
72. Liu, F.; Jia, B.; Chen, B.; Geng, W. Moisture Transfer in Building Envelope and Influence on Heat Transfer. *Procedia Eng.* **2017**, *205*, 3654–3661. [[CrossRef](#)]
73. Wang, X.; Jin, X.; Yin, Y.; Shi, X.; Zhou, X. A Transient Heat and Moisture Transfer Model for Building Materials Based on Phase Change Criterion under Isothermal and Non-Isothermal Conditions. *Energy* **2021**, *224*, 120112. [[CrossRef](#)]
74. CEN/TC 89/WG 10—Moisture. Available online: <https://standards.iteh.ai/catalog/tc/cen/827dd119-af0f-4d12-a371-3d0f0008b295/cen-tc-89-wg-10> (accessed on 31 July 2023).
75. Carl-Eric, H.; Olaf, A.; Bijan, A.-Z.; Rachel, B.; Harold, B.; Jan, C.; Reda, D.; Max, F.; John, G.; Hugo, H.; et al. Assessment Method of Numerical Prediction Models for Combined Heat, Air and Moisture Transfer in Building Components: Benchmarks for One-Dimensional Cases. *J. Therm. Envel. Build. Sci.* **2004**, *27*, 327–352. [[CrossRef](#)]
76. Janssen, H.; Blocken, B.; Carmeliet, J. Conservative Modelling of the Moisture and Heat Transfer in Building Components under Atmospheric Excitation. *Int. J. Heat Mass Transf.* **2007**, *50*, 1128–1140. [[CrossRef](#)]
77. Li, Q.; Rao, J.; Fazio, P. Development of HAM Tool for Building Envelope Analysis. *Build. Environ.* **2009**, *44*, 1065–1073. [[CrossRef](#)]
78. Fang, A.; Chen, Y.; Wu, L. Modeling and Numerical Investigation for Hygrothermal Behavior of Porous Building Envelope Subjected to the Wind Driven Rain. *Energy Build.* **2021**, *231*, 110572. [[CrossRef](#)]
79. Fang, A.; Chen, Y.; Wu, L. Transient Simulation of Coupled Heat and Moisture Transfer through Multi-Layer Walls Exposed to Future Climate in the Hot and Humid Southern China Area. *Sustain. Cities Soc.* **2020**, *52*, 101812. [[CrossRef](#)]
80. Odgaard, T.; Bjarløv, S.P.; Rode, C. Influence of Hydrophobation and Deliberate Thermal Bridge on Hygrothermal Conditions of Internally Insulated Historic Solid Masonry Walls with Built-in Wood. *Energy Build.* **2018**, *173*, 530–546. [[CrossRef](#)]
81. Remki, B.; Abahri, K.; Tahlaoui, M.; Belarbi, R. Hygrothermal Transfer in Wood Drying under the Atmospheric Pressure Gradient. *Int. J. Therm. Sci.* **2012**, *57*, 135–141. [[CrossRef](#)]
82. Berger, J.; Dutykh, D.; Mendes, N.; Rysbaiuly, B. A New Model for Simulating Heat, Air and Moisture Transport in Porous Building Materials. *Int. J. Heat Mass Transf.* **2019**, *134*, 1041–1060. [[CrossRef](#)]
83. Ayres de Mello, L.; Moura, L.M.; Mendes, N. A Model for Predicting Heat, Air and Moisture Transfer through Fibrous Materials. *Int. J. Therm. Sci.* **2019**, *145*, 106036. [[CrossRef](#)]
84. Ayres de Mello, L.; Moura, L.M.; Mendes, N. A Model for Assessment of Heat and Moisture Transfer through Hollow Porous Buildings Elements. *Case Stud. Therm. Eng.* **2019**, *14*, 100446. [[CrossRef](#)]
85. Sawadogo, M.; Benmahiddine, F.; Godin, A.; Duquesne, M.; Belarbi, R.; Hamami, A. Development and Hygrothermal Performance Analysis of a Novel Eco-Friendly Insulating Wall under Various Climatic Conditions. *Build. Environ.* **2023**, *245*, 110841. [[CrossRef](#)]
86. Nagata, G.A.; Costa, T.V.; Perazzini, M.T.B.; Perazzini, H. Coupled Heat and Mass Transfer Modelling in Convective Drying of Biomass at Particle-Level: Model Validation with Experimental Data. *Renew. Energy* **2020**, *149*, 1290–1299. [[CrossRef](#)]
87. Qin, M.; Belarbi, R.; Ait-Mokhtar, A.; Nilsson, L.-O. Nonisothermal Moisture Transport in Hygroscopic Building Materials: Modeling for the Determination of Moisture Transport Coefficients. *Transp. Porous. Med.* **2008**, *72*, 255–271. [[CrossRef](#)]
88. Zhai, Z.; Chen, Q.; Haves, P.; Klems, J.H. On Approaches to Couple Energy Simulation and Computational Fluid Dynamics Programs. *Build. Environ.* **2002**, *37*, 857–864. [[CrossRef](#)]
89. Kwiatkowski, J.; Woloszyn, M.; Roux, J.-J. Influence of Sorption Isotherm Hysteresis Effect on Indoor Climate and Energy Demand for Heating. *Appl. Therm. Eng.* **2011**, *31*, 1050–1057. [[CrossRef](#)]
90. Ferroukhi, M.Y.; Djedjig, R.; Limam, K.; Belarbi, R. Hygrothermal Behavior Modeling of the Hygroscopic Envelopes of Buildings: A Dynamic Co-Simulation Approach. *Build. Simul.* **2016**, *9*, 501–512. [[CrossRef](#)]
91. Ferroukhi, M.Y.; Djedjig, R.; Belarbi, R.; Limam, K.; Abahri, K. Effect of Coupled Heat, Air and Moisture Transfers Modeling in the Wall on the Hygrothermal Behavior of Buildings. *Energy Procedia* **2015**, *78*, 2584–2589. [[CrossRef](#)]

92. Ferroukhi, M.Y.; Abahri, K.; Belarbi, R.; Limam, K. Integration of a Hygrothermal Transfer Model for Envelope in a Building Energy Simulation Model: Experimental Validation of a HAM–BES Co-Simulation Approach. *Heat Mass Transfer* **2017**, *53*, 1851–1861. [CrossRef]
93. Frasca, F.; Verticchio, E.; Cornaro, C.; Siani, A.M. Performance Assessment of Hygrothermal Modelling for Diagnostics and Conservation in an Italian Historical Church. *Build. Environ.* **2021**, *193*, 107672. [CrossRef]
94. Alvarado-Alvarado, A.A.; De Bock, A.; Ysebaert, T.; Belmans, B.; Denys, S. Modeling the Hygrothermal Behavior of Green Walls in Comsol Multiphysics®: Validation against Measurements in a Climate Chamber. *Build. Environ.* **2023**, *238*, 110377. [CrossRef]
95. Blocken, B.; Carmeliet, J. Spatial and Temporal Distribution of Driving Rain on a Low-Rise Building. *Wind. Struct. Int. J.* **2002**, *5*, 441–462. [CrossRef]
96. Yu, S.; Liu, X.; Li, Y.; He, S.; Yao, Y.; Sun, S. Experimental and Numerical Simulation Study on Hygrothermal Migration of Damaged Envelope Walls during Wind-Driven Rain. *Build. Environ.* **2023**, *243*, 110653. [CrossRef]
97. EN 15026; Hygrothermal Performance of Building Components and Elements—Assessment of Moisture Transfer by Numerical Simulation. British Standards: London, UK, 2007.
98. Judkoff, R.; Neymark, J. *International Energy Agency Building Energy Simulation Test (BESTEST) and Diagnostic Method*; National Renewable Energy Lab. (NREL): Golden, CO, USA, 1995.
99. Van Schijndel, A.W.M.; Goesten, S.; Schellen, H.L. Simulating the Complete HAMSTAD Benchmark Using a Single Model Implemented in Comsol. *Energy Procedia* **2017**, *132*, 429–434. [CrossRef]
100. Shen, X.; Li, L.; Cui, W.; Feng, Y. Coupled Heat and Moisture Transfer in Building Material with Freezing and Thawing Process. *J. Build. Eng.* **2018**, *20*, 609–615. [CrossRef]
101. Chen, G.; Luo, Q.; Guo, X.; Liu, X.; Tu, M.; He, Y. Study on Mould Germination Risk in Hygroscopic Building Wall. *Procedia Eng.* **2017**, *205*, 2712–2719. [CrossRef]
102. Knarud, J.I.; Geving, S. Implementation and Benchmarking of a 3D Hygrothermal Model in the COMSOL Multiphysics Software. *Energy Procedia* **2015**, *78*, 3440–3445. [CrossRef]
103. Wan, H.; Huang, G.; Xu, X. Development of a Moisture Transfer Calculation Method of Hygroscopic Material Plate in Buildings. *Build. Environ.* **2018**, *142*, 398–413. [CrossRef]
104. Korjenic, A.; Bednar, T. An Analytical Solution of a Moisture Transfer Problem for Coupled Room and Building Component. *Energy Build.* **2012**, *47*, 254–259. [CrossRef]
105. COMSOL: Multiphysics Software for Optimizing Designs. Available online: <https://www.comsol.com/> (accessed on 4 August 2023).
106. Liu, X.; Chen, Y.; Ge, H.; Fazio, P.; Chen, G. Numerical Investigation for Thermal Performance of Exterior Walls of Residential Buildings with Moisture Transfer in Hot Summer and Cold Winter Zone of China. *Energy Build.* **2015**, *93*, 259–268. [CrossRef]
107. WUFI. Available online: <https://www.wufi.de/> (accessed on 6 December 2023).
108. Huang, Z.; Sun, Y.; Musso, F. Hygrothermal Performance Optimization on Bamboo Building Envelope in Hot-Humid Climate Region. *Constr. Build. Mater.* **2019**, *202*, 223–245. [CrossRef]
109. Park, J.H.; Kang, Y.; Lee, J.; Chang, S.J.; Wi, S.; Kim, S. Development of Wood-Lime Boards as Building Materials Improving Thermal and Moisture Performance Based on Hygrothermal Behavior Evaluation. *Constr. Build. Mater.* **2019**, *204*, 576–585. [CrossRef]
110. López, O.; Torres, I.; Guimarães, A.S.; Delgado, J.M.P.Q.; de Freitas, V.P. Inter-Laboratory Variability Results of Porous Building Materials Hygrothermal Properties. *Constr. Build. Mater.* **2017**, *156*, 412–423. [CrossRef]
111. Luisa, S.; Andreas, N.; Stefan, V. *Validierung der Solverimplementierung des Hygrothermischen Simulationsprogramms Delphin*; Technische Universität Dresden: Dresden, Germany, 2013.
112. Ruiz, M.; Masson, V.; Bonhomme, M.; Ginestet, S. Numerical Method for Solving Coupled Heat and Mass Transfer through Walls for Future Integration into an Urban Climate Model. *Build. Environ.* **2023**, *231*, 110028. [CrossRef]
113. Gonçalves, M.; Simões, N.; Serra, C.; Flores-Colen, I. Laboratory Assessment of the Hygrothermal Performance of an External Vacuum-Insulation Composite System. *Energy Build.* **2022**, *254*, 111549. [CrossRef]
114. Pavlík, Z.; Černý, R. Experimental Assessment of Hygrothermal Performance of an Interior Thermal Insulation System Using a Laboratory Technique Simulating On-Site Conditions. *Energy Build.* **2008**, *40*, 673–678. [CrossRef]
115. Wu, D.; Rahim, M.; El Ganaoui, M.; Bennacer, R.; Djedjig, R.; Liu, B. Dynamic Hygrothermal Behavior and Energy Performance Analysis of a Novel Multilayer Building Envelope Based on PCM and Hemp Concrete. *Constr. Build. Mater.* **2022**, *341*, 127739. [CrossRef]
116. Talukdar, P.; Olutmayin, S.O.; Osanyintola, O.F.; Simonson, C.J. An Experimental Data Set for Benchmarking 1-D, Transient Heat and Moisture Transfer Models of Hygroscopic Building Materials. Part I: Experimental Facility and Material Property Data. *Int. J. Heat Mass Transf.* **2007**, *50*, 4527–4539. [CrossRef]
117. Olutmayin, S.O.; Simonson, C.J. Measuring and Modeling Vapor Boundary Layer Growth during Transient Diffusion Heat and Moisture Transfer in Cellulose Insulation. *Int. J. Heat Mass Transf.* **2005**, *48*, 3319–3330. [CrossRef]
118. Van Belleghem, M.; Steeman, M.; Willockx, A.; Janssens, A.; De Paepe, M. Benchmark Experiments for Moisture Transfer Modelling in Air and Porous Materials. *Build. Environ.* **2011**, *46*, 884–898. [CrossRef]
119. Evrard, A.; De Herde, A. Hygrothermal Performance of Lime-Hemp Wall Assemblies. *J. Build. Phys.* **2010**, *34*, 5–25. [CrossRef]

120. Colinart, T.; Lelievre, D.; Glouannec, P. Experimental and Numerical Analysis of the Transient Hygrothermal Behavior of Multilayered Hemp Concrete Wall. *Energy Build.* **2016**, *112*, 1–11. [[CrossRef](#)]
121. Boukhelf, F.; Trabelsi, A.; Belarbi, R.; Bachir Bouiadjra, M. Experimental and Numerical Modelling of Hygrothermal Transfer: Application on Building Energy Performance. *Energy Build.* **2022**, *254*, 111633. [[CrossRef](#)]
122. Belloum, R.; Agoudjil, B.; Chennouf, N.; Boudenne, A. Hygrothermal Performance Assessment of a Bio-Based Building Made with Date Palm Concrete Walls. *Build. Environ.* **2022**, *223*, 109467. [[CrossRef](#)]
123. Chennouf, N.; Agoudjil, B.; Alioua, T.; Boudenne, A.; Benzarti, K. Experimental Investigation on Hygrothermal Performance of a Bio-Based Wall Made of Cement Mortar Filled with Date Palm Fibers. *Energy Build.* **2019**, *202*, 109413. [[CrossRef](#)]
124. Rahim, M.; Djedjig, R.; Wu, D.; Bennacer, R.; Ganaoui, M.E. Experimental Investigation of Hygrothermal Behavior of Wooden-Frame House under Real Climate Conditions. *Energy Built Environ.* **2023**, *4*, 122–129. [[CrossRef](#)]
125. Zhan, Q.; Pungercar, V.; Musso, F.; Ni, H.; Xiao, Y. Hygrothermal Investigation of Lightweight Steel-Framed Wall Assemblies in Hot-Humid Climates: Measurement and Simulation Validation. *J. Build. Eng.* **2021**, *42*, 103044. [[CrossRef](#)]
126. Friis, N.K.; Møller, E.B.; Lading, T. Hygrothermal Assessment of External Walls in Arctic Climates: Field Measurements and Simulations of a Test Facility. *Build. Environ.* **2023**, *238*, 110347. [[CrossRef](#)]
127. Stefan, J. Über einige probleme der theorie der wärmeleitung. *Sitzungber. Wien Akad. Mat. Natur.* **1889**, *98*, 473–484.
128. Alexiades, V. *Mathematical Modeling of Melting And Freezing Processes*; CRC Press: Boca Raton, FL, USA, 1992; ISBN 978-1-56032-125-5.
129. Eyres, N.R.; Hartree, D.R.; Ingham, J.; Sarjant, R.J.; Wagstaff, J.B. The Calculation of Variable Heat Flow in Solids. *Philos. Trans. R. Soc. Lond. Ser. A Math. Phys. Sci.* **1946**, *240*, 1–57. [[CrossRef](#)]
130. Swaminathan, C.R.; Voller, V.R. On the Enthalpy Method. *Int. J. Numer. Methods Heat Fluid Flow* **1993**, *3*, 233–244. [[CrossRef](#)]
131. Voller, V.R. An Overview of Numerical Methods for Solving Phase Change Problems. *Adv. Numer. Heat Transf.* **1997**, *1*, 341–380.
132. Hashemi, H.T.; Sliepcevich, C.M. A Numerical Method for Solving Two-Dimensional Problems of Heat Conduction with Change of Phase. *Chem. Eng. Prog. Symp. Series* **1967**, *63*, 34–41.
133. Günther, E.; Hiebler, S.; Mehling, H.; Redlich, R. Enthalpy of Phase Change Materials as a Function of Temperature: Required Accuracy and Suitable Measurement Methods. *Int. J. Thermophys.* **2009**, *30*, 1257–1269. [[CrossRef](#)]
134. Bonacina, C.; Comini, G.; Fasano, A.; Primicerio, M. Numerical Solution of Phase-Change Problems. *Int. J. Heat Mass Transf.* **1973**, *16*, 1825–1832. [[CrossRef](#)]
135. Morgan, K.; Lewis, R.W.; Zienkiewicz, O.C. An improved algorithm for heat conduction problems with phase change. *Int. J. Numer. Methods Eng.* **1978**, *12*, 1191–1195. [[CrossRef](#)]
136. Poirier, D.; Salcudean, M. On Numerical Methods Used in Mathematical Modeling of Phase Change in Liquid Metals. *J. Heat Transf.* **1988**, *110*, 562–570. [[CrossRef](#)]
137. Han, X.X.; Tian, Y.; Zhao, C.Y. An Effectiveness Study of Enhanced Heat Transfer in Phase Change Materials (PCMs). *Int. J. Heat Mass Transf.* **2013**, *60*, 459–468. [[CrossRef](#)]
138. Ghoneim, A.Y. A Smoothed Particle Hydrodynamics-Phase Field Method with Radial Basis Functions and Moving Least Squares for Meshfree Simulation of Dendritic Solidification. *Appl. Math. Model.* **2020**, *77*, 1704–1741. [[CrossRef](#)]
139. Shen, Y.; Liu, S.; Zeng, C.; Zhang, Y.; Li, Y.; Han, X.; Yang, L.; Yang, X. Experimental Thermal Study of a New PCM-Concrete Thermal Storage Block (PCM-CTSB). *Constr. Build. Mater.* **2021**, *293*, 123540. [[CrossRef](#)]
140. Dehmous, M.; Franquet, E.; Lamrous, N. Mechanical and Thermal Characterizations of Various Thermal Energy Storage Concretes Including Low-Cost Bio-Sourced PCM. *Energy Build.* **2021**, *241*, 110878. [[CrossRef](#)]
141. Jia, C.; Geng, X.; Liu, F.; Gao, Y. Thermal Behavior Improvement of Hollow Sintered Bricks Integrated with Both Thermal Insulation Material (TIM) and Phase-Change Material (PCM). *Case Stud. Therm. Eng.* **2021**, *25*, 100938. [[CrossRef](#)]
142. Hamidi, Y.; Aketouane, Z.; Malha, M.; Bruneau, D.; Bah, A.; Goiffon, R. Integrating PCM into Hollow Brick Walls: Toward Energy Conservation in Mediterranean Regions. *Energy Build.* **2021**, *248*, 111214. [[CrossRef](#)]
143. Li, M.; Cao, Q.; Pan, H.; Wang, X.; Lin, Z. Effect of Melting Point on Thermodynamics of Thin PCM Reinforced Residential Frame Walls in Different Climate Zones. *Appl. Therm. Eng.* **2021**, *188*, 116615. [[CrossRef](#)]
144. Frazzica, A.; Brancato, V.; Palomba, V.; La Rosa, D.; Grungo, F.; Calabrese, L.; Proverbio, E. Thermal Performance of Hybrid Cement Mortar-PCMs for Warm Climates Application. *Sol. Energy Mater. Sol. Cells* **2019**, *193*, 270–280. [[CrossRef](#)]
145. Zhou, D.; Shire, G.S.F.; Tian, Y. Parametric Analysis of Influencing Factors in Phase Change Material Wallboard (PCMW). *Appl. Energy* **2014**, *119*, 33–42. [[CrossRef](#)]
146. Thiele, A.M.; Sant, G.; Pilon, L. Diurnal Thermal Analysis of Microencapsulated PCM-Concrete Composite Walls. *Energy Convers. Manag.* **2015**, *93*, 215–227. [[CrossRef](#)]
147. Jia, J.; Liu, B.; Ma, L.; Wang, H.; Li, D.; Wang, Y. Energy Saving Performance Optimization and Regional Adaptability of Prefabricated Buildings with PCM in Different Climates. *Case Stud. Therm. Eng.* **2021**, *26*, 101164. [[CrossRef](#)]
148. Al-Absi, Z.A.; Mohd Isa, M.H.; Ismail, M. Phase Change Materials (PCMs) and Their Optimum Position in Building Walls. *Sustainability* **2020**, *12*, 1294. [[CrossRef](#)]
149. Wi, S.; Chang, S.J.; Kim, S. Improvement of Thermal Inertia Effect in Buildings Using Shape Stabilized PCM Wallboard Based on the Enthalpy-Temperature Function. *Sustain. Cities Soc.* **2020**, *56*, 102067. [[CrossRef](#)]
150. Shi, X.; Memon, S.A.; Tang, W.; Cui, H.; Xing, F. Experimental Assessment of Position of Macro Encapsulated Phase Change Material in Concrete Walls on Indoor Temperatures and Humidity Levels. *Energy Build.* **2014**, *71*, 80–87. [[CrossRef](#)]

151. Chang, S.J.; Kang, Y.; Wi, S.; Jeong, S.-G.; Kim, S. Hygrothermal Performance Improvement of the Korean Wood Frame Walls Using Macro-Packed Phase Change Materials (MPPCM). *Appl. Therm. Eng.* **2017**, *114*, 457–465. [[CrossRef](#)]
152. Zhu, N.; Li, X.; Hu, P.; Lei, F.; Wei, S.; Wang, W. An Exploration on the Performance of Using Phase Change Humidity Control Material Wallboards in Office Buildings. *Energy* **2022**, *239*, 122433. [[CrossRef](#)]
153. Wu, Z.; Qin, M.; Zhang, M. Phase Change Humidity Control Material and Its Impact on Building Energy Consumption. *Energy Build.* **2018**, *174*, 254–261. [[CrossRef](#)]
154. Benmahiddine, F. Études des transferts couplés de chaleur, d'air et d'humidité par des techniques de changement d'échelle (microscopique-macroscopique): Application à L'évaluation de la Performance Energétique et la Durabilité des Matériaux de Construction. Ph.D. Thesis, Université de La Rochelle, La Rochelle, France, 2020.
155. CEN, EN ISO 12572; Hygrothermal Performance of Building Materials and Products—Determination of Water Vapour Transmission Properties. International Standards Organization: Geneva, Switzerland, 2001.
156. Oubrahim, I. *Fiabilisation des Approches Théoriques Pour la Caractérisation des Matériaux et la Modélisation Hygrothermique des Enveloppes du Bâtiment*; Université de La Rochelle: La Rochelle, France, 2023.
157. Kaemmerlen, A. Transfert de Chaleur à Travers Les Isolants Thermiques Du Bâtiment. Ph.D. Thesis, Université Henri Poincaré, Nancy, France, 2009.
158. Sawadogo, M.; Godin, A.; Duquesne, M.; Lacroix, E.; Veillère, A.; Hamami, A.E.A.; Belarbi, R. Investigation of Eco-Friendly and Economic Shape-Stabilized Composites for Building Walls and Thermal Comfort. *Build. Environ.* **2023**, *231*, 110026. [[CrossRef](#)]
159. Sawadogo, M.; Benmahiddine, F.; Hamami, A.E.A.; Belarbi, R.; Godin, A.; Duquesne, M. Investigation of a Novel Bio-Based Phase Change Material Hemp Concrete for Passive Energy Storage in Buildings. *Appl. Therm. Eng.* **2022**, *212*, 118620. [[CrossRef](#)]
160. Duquesne, M.; Mailhé, C.; Doppiu, S.; Dauvergne, J.-L.; Santos-Moreno, S.; Godin, A.; Fleury, G.; Rouault, F.; Palomo del Barrio, E. Characterization of Fatty Acids as Biobased Organic Materials for Latent Heat Storage. *Materials* **2021**, *14*, 4707. [[CrossRef](#)] [[PubMed](#)]
161. Mailhé, C.; Duquesne, M.; Palomo del Barrio, E.; Azaiez, M.; Achchaq, F. Phase Diagrams of Fatty Acids as Biosourced Phase Change Materials for Thermal Energy Storage. *Appl. Sci.* **2019**, *9*, 1067. [[CrossRef](#)]

Disclaimer/Publisher's Note: The statements, opinions and data contained in all publications are solely those of the individual author(s) and contributor(s) and not of MDPI and/or the editor(s). MDPI and/or the editor(s) disclaim responsibility for any injury to people or property resulting from any ideas, methods, instructions or products referred to in the content.